Balanced Input from the tRNA Prenyltransferase MiaA Controls the Stress Resistance and Virulence Potential of Extraintestinal Pathogenic *Escherichia coli*

Matthew G. Blango*†◊, Brittany A. Fleming*†, William M. Kincannon‡, Alex Tran*, Adam J. Lewis*, Colin W. Russell*, Qin Zhou*, Lisa M. Baird§, John R. Brannon¶, Connor J. Beebout¶, Vahe Bandarian‡, Maria Hadjifraniskou¶, Michael T. Howard§, and Matthew A. Mulvey*#

*Division of Microbiology and Immunology, Pathology Department, University of Utah School of Medicine, Salt Lake City, Utah.

‡Department of Chemistry, University of Utah, Salt Lake City, Utah.

§Department of Human Genetics, University of Utah, Salt Lake City, Utah.

¶Department of Pathology, Microbiology, and Immunology, Vanderbilt University Medical Center, Nashville, Tennessee.

◊Current address: Junior Research Group RNA Biology of Fungal Infections, Leibniz Institute for Natural Product Research and Infection Biology (Leibniz-HKI), Jena, Germany.

†These authors contributed equally to the work. Listed alphabetically.

#Corresponding author:
Phone: 801-581-5967
E-mail: mulvey@path.utah.edu

ABSTRACT

An ability to adapt to rapidly changing and often hostile environments is key to the success of many bacterial pathogens. In *Escherichia coli*, the highly conserved enzymes MiaA and MiaB mediate the sequential prenylation and methylthiolation of adenosine-37 within tRNAs that decode UNN codons. Here, we show that MiaA, but not MiaB, is critical to the fitness and virulence of extraintestinal pathogenic *E. coli* (ExPEC), a major cause of urinary tract and bloodstream infections. Deletion of *miaA* has pleiotropic effects, rendering ExPEC especially sensitive to stressors like nitrogen and oxygen radicals and osmotic shock. We find that stress can stimulate striking changes in *miaA* expression, which in turn can increase translational frameshifting and markedly alter the bacterial proteome. Cumulatively, these data indicate that ExPEC, and likely other organisms, can vary MiaA levels as a means to fine-tune translation and the spectrum of expressed proteins in response to changing environmental challenges.

INTRODUCTION

The translation of mRNA into protein by ribosomes and aminoacyl-transfer RNA (tRNA) complexes is an energy-intensive process that is subject to multiple levels of complicated regulation. For example, tRNAs can be covalently modified by more than 100 different moieties that can influence the charging of tRNAs with amino acids, tRNA stability, codon usage, and reading frame maintenance [1-4]. In *Escherichia coli* and other bacteria, the hypomodification of tRNAs can result in decreased growth rates, altered metabolic requirements, and reduced stress resistance [5-8]. Loss of tRNA modifications can also impact the fitness and virulence potential of many important bacterial pathogens, including *Streptomyces pyogenes*, *Pseudomonas spp.*, *Shigella flexneri*, *Agrobacterium tumefaciens, Mycobacterium tuberculosis, Aeromonas hydrophila*, *Streptococcus spp.*, and *Salmonella enterica* serotype Typhimurium [6, 9-21]. Together, these findings suggest that tRNA modification serves as a regulatory nexus that can control a wide array of bacterial activities.

One of the most commonly modified tRNA residues in bacteria is adenosine-37 (A-37), which lies adjacent to the anticodon loop [8, 22]. In its final form in *E. coli*, A-37 of UNN-recognizing tRNA molecules is oftentimes prenylated and methylthiolated [23]. The *miaA* gene of *E. coli* encodes a tRNA prenyltransferase that catalyzes the addition of a prenyl group onto the N^6-nitrogen of A-37 to create i^6A-37 tRNA [24, 25] (**Fig. 1A**). The modified i^6A-37 residue is subsequently methylthiolated by the radical-S-adenosylmethionine enzyme MiaB to create ms^2i^6A-37 [26]. The bulky and hydrophobic ms^2i^6A-37 modification enhances tRNA interactions with UNN target codons, promoting reading frame maintenance and translational fidelity [5, 8, 27]. Mutations in the *miaA* locus

result in an unmodified A-37 residue, as prenylation is required for methylthiolation by MiaB. In K-12 laboratory-adpated *E. coli* strains, mutations in *miaA* impair attenuation of the tryptophan and phenylalanine operons [28, 29] and diminish translation of the stationary phase sigma factor RpoS and the small RNA chaperone Hfq [7, 30, 31]. Additionally, mutants lacking *miaA* are unable to effectively resolve aberrant DNA-protein crosslinks [32] and have somewhat elevated spontaneous mutation frequencies [33-35]. The ms^2i^6A-37 modification is highly conserved in both prokaryotes and eukaryotes, though the specific enzymes that mediate this modification have diverged within evolutionarily distant organisms [8]. However, in prokaryotes, MiaA and MiaB homologues are relatively well conserved, and the enzymes appear to function similarly in all tested bacterial species [36, 37].

Given that the ms^2i^6A-37 modification is a well-defined regulator of many tRNA functions in lab-adapted K-12 *E. coli* strains, we sought to understand how this modification is co-opted in a pathogenic *E. coli* background. *E. coli* pathotypes display extensive genetic diversity and are usually more resilient under stress than their lab-adapted counterparts [38]. Extraintestinal Pathogenic *E. coli* (ExPEC) typically reside in the lower intestinal tract of mammals, where they are rarely associated with pathology [39]. However, when they spread outside the gut to other host sites ExPEC can cause a number of serious diseases, including urinary tract and bloodstream infections [38, 40]. Bacterial pathogens like ExPEC must be able to rapidly respond to a diverse array of stressors encountered within changing host environments. These include nutrient deprivation, redox stress in the form of oxygen and nitrogen radicals, extremes in pH,

envelope damage, changing osmotic pressures, and a wide assortment of host immune effector cells and antimicrobial compounds [41-45].

Shifts in the prevalence of specific tRNA modifications, such as A-37 prenylation mediated by MiaA, are proposed to help optimize bacterial responses to stress by affecting translational fidelity and selective protein expression [14, 33, 46]. In other words, changing levels of tRNA modifications may control the codon-biased translation of select transcripts, providing a post-transcriptional programmable mechanism that distressed cells can use to facilitate beneficial changes in their proteomes. Here we provide evidence in support of this hypothesis, showing that ExPEC can modulate MiaA levels in response to stress, and that varying levels of this enzyme can increase translational frameshifting and markedly alter the spectrum of expressed proteins. Furthermore, our data reveal that MiaA, but not MiaB, is critical to the fitness and virulence of ExPEC in both *in vitro* assays and in mouse models of infection and intestinal colonization.

RESULTS

MiaA promotes ExPEC fitness and virulence in vivo

To assess the importance of MiaA and MiaB for ExPEC within varied host environments, we employed well-established mouse models of gut colonization, urinary tract infection (UTI), and bloodstream infection [47]. For these and subsequent experiments, *miaA* and *miaB* were independently deleted from the ExPEC reference strain UTI89 to generate the isogenic knockout mutants UTI89Δ*miaA* and UTI89Δ*miaB* [48, 49].

Gut colonization. The mammalian gastrointestinal (GI) tract serves as a major reservoir for ExPEC that can seed extraintestinal infections [50-54]. Roles for MiaA and MiaB in ExPEC colonization of the GI tract were probed using competitive assays in which ~10^9 colony forming units (CFU) of a 1:1 mixture of UTI89 and either UTI89Δ*miaA* or UTI89Δ*miaB* were introduced into adult specific-pathogen-free (SPF) BALB/c mice via intragastric gavage [55-57]. In this model system, the levels of ExPEC recovered from the feces reflect ExPEC titers within the large intestines [55]. For these assays, UTI89 and the *miaA* and *miaB* knockout mutants were engineered to express either kanamycin (Kan^R) or chloramphenicol (Cam^R) resistance cassettes so that the strains could be readily identified by plating fecal homogenates on selective media. Feces were collected at the indicated time points and the numbers of viable bacteria were enumerated to determine competitive indices (CI). UTI89Δ*miaA* was significantly outcompeted by wild-type UTI89 as early as day 3 post-inoculation (**Fig. 1B**). By day 10, there was about a 25,000-fold reduction in the relative levels of UTI89Δ*miaA* recovered from the feces, correlating with a median CI of -4.39. At this time point, UTI89Δ*miaA* titers in the majority of mice were below the limit of detection. In contrast, there were no notable differences in titers between UTI89Δ*miaB* and UTI89 in the feces at any time point (**Fig. 1C**). These results indicate that the loss of MiaA, but not MiaB, greatly impairs the fitness of UTI89 within the gut

UTI. During the course of a UTI, ExPEC is able to bind and invade the host epithelial cells that comprise the bladder mucosa [58]. Once internalized into bladder cells, ExPEC can traffic into late endosome-like compartments where it may form quiescent reservoir populations that promote long-term bacterial persistence.

Alternatively, ExPEC can enter the host cytosol and rapidly multiply, forming large intracellular bacterial communities that eventually rupture the epithelial cell. In cell culture-based assays using a bladder epithelial cell line, we found that UTI89Δ*miaA* and UTI89Δ*miaB* are able to bind, invade, and survive intracellularly in overnight assays much like wild-type UTI89 (**Supplemental Fig. S1**).

To investigate MiaA and MiaB requirements during UTI, 10^7 CFU of wild-type UTI89, UTI89Δ*miaA*, and UTI89Δ*miaB* were independently inoculated via transurethral catheterization into adult female CBA/J mice and bacterial titers in the bladders were determined after 3 days. In this analysis, UTI89Δ*miaB* showed no statistically significant defect relative to the parent strain; whereas the Δ*miaA* strain was clearly attenuated (**Fig. 1D**). Deficiencies in bladder colonization by UTI89Δ*miaA* were apparent by 6 h post-inoculation (**Supplemental Fig. S2A**), and were still significant after 9 days (**Supplemental Fig. S2B**). The differences observed between wild-type UTI89 and UTI89Δ*miaA* at 3 days post-inoculation of CBA/J mice were also manifest in C3H/HeJ mice (**Supplemental Fig. S2C**). Due to defects in Toll-like receptor 4 (TLR4) signaling and other innate defenses, C3H/HeJ mice have attenuated inflammatory responses and increased susceptibility to UTI [59-62]. Our results indicate that the decreased capacity of UTI89Δ*miaA* to colonize the bladder is not attributable to an inability of the *miaA* knockout to handle TLR4-dependent innate host defenses. Collectively, these results indicate that MiaA is required for maximal fitness in mouse UTI models, while MiaB is less critical.

Bloodstream infection. ExPEC is a leading cause of bloodstream infections, which too often trigger discordant systemic inflammatory responses that can result in a life-

threatening condition known as sepsis [63]. To examine the contributions of MiaA and MiaB to ExPEC virulence and fitness in a model of sepsis, adult C57Bl/6 mice were inoculated via intraperitoneal (i.p.) injections with ~10^7 CFU of wild-type UTI89, UTI89Δ*miaA*, or UTI89Δ*miaB.* Following i.p. injection, the bacteria enter the bloodstream and disseminate [56, 64, 65]. In our experiments, only 15% (2/13) of the mice infected with wild-type UTI89, and 0% (0/13) of the mice injected with UTI89Δ*miaB,* were viable after 48 hours (**Fig. 1E**). In sharp contrast, 84% (11/13) of the mice infected with UTI89Δ*miaA* survived. At six hours post-injection, significantly lower numbers of bacteria were recovered from the spleens and kidneys of UTI89Δ*miaA*-infected mice, relative to mice infected with wild-type UTI89 or UTI89Δ*miaB* (**Supplemental Fig. S3A and B**). While not significant, titers in the liver also trended lower in UTI89Δ*miaA*-infected mice (**Supplemental Fig. S3C**). Combined, these data demonstrate that MiaA is important for the virulence of ExPEC and its survival during systemic infections, while MiaB appears dispensable.

MiaA enhances ExPEC growth and stress resistance

Earlier studies showed that K-12 *E. coli* and *Salmonella* mutants lacking *miaA* are moderately impaired in nutrient-rich broth, but less so in nutrient-limited media [27, 35, 66]. Using *in vitro* growth assays, we found that UTI89Δ*miaA* grew normally in modified M9 minimal media, but failed to reach densities as high as the wild-type strain in more complex, nutrient-rich lysogeny broth (LB) (**Fig. 2A and B**). In contrast, the *miaB* knockout exhibited no overt growth defects in either type of media. These data suggest that UTI89Δ*miaA* has reduced metabolic flexibility relative to wild-type UTI89 and the *miaB*

mutant. This may contribute to the decreased fitness of UTI89Δ*miaA* in our mouse models, where the bacteria likely encounter marked shifts in nutrient availability. However, within different host environments ExPEC will face a wide variety of additional challenges that might be countered by MiaA-dependent processes. We investigated this possibility by examining the effects of MiaA and MiaB on ExPEC resistance to nitrosative, oxidative, and osmotic stress.

Oxidative and nitrosative stress. During the course of an infection, both host and bacterial cells can produce reactive oxygen and nitrogen radicals that can damage lipids, proteins, and nucleic acids [67, 68]. The contributions of MiaA and MiaB to nitrosative and oxidative stress resistance were assessed using acidified sodium nitrite (ASN) and methyl viologen (MV), respectively. When added to low pH morpholineethanesulfonic acid (MES)-buffered LB (MES-LB; pH 5.0), sodium nitrite dismutates to form nitrous acid which in turn generates NO and other harmful reactive nitrogen species [69]. In un-supplemented MES-LB, UTI89Δ*miaA* reached a lower maximal density than wild-type UTI89 (**Fig. 2C**), similar to results obtained using standard LB (**Fig. 2B**). The addition 1 mM ASN delayed entry of UTI89Δ*miaA* into exponential growth phase by close to 4 hours (**Fig. 2D**), while 2 mM ASN delayed growth by more than 15 hours relative to wild-type UTI89 (**Fig. 2E**). The addition of 1 mM MV, which produces superoxide radicals [70], had even stronger inhibitory effects on growth of UTI89Δ*miaA* (**Fig. 2F**). In contrast, UTI89Δ*miaB* grew much like the wild-type strain in the presence of ASN or MV (**Fig. 2D-F**). Complementation with pMiaA$_{nat}$, a low copy plasmid that encodes MiaA under control of its native promoter, restored growth of UTI89Δ*miaA* to near wild-type levels in both 2 mM ASN (**Fig. 2G**) and in 1 mM MV (**Fig. 2H**).

178 *Osmotic stress*. During a UTI, osmotic pressure within the bladder can shift from
179 50 to >1,400 mOsm/kg due to varying concentrations of solutes like sodium and urea [71,
180 72]. By comparison, the normal osmolarity of blood ranges from about 275 to 295
181 mOsm/kg. To test the sensitivities of wild-type UTI89 and the knockout strains to
182 hypoosmotic stress, we diluted the bacteria from early stationary phase cultures into
183 ddH_2O, and then quantified the number of viable bacteria every 30 minutes over the
184 course of 2 hours. Titers of UTI89Δ*miaA* carrying the empty vector pACYC184 were
185 greatly reduced following exposure to hypoosmotic stress, whereas the levels of
186 UTI89/pACYC184 and UTI89Δ*miaB*/pACYC184 remained mostly unchanged (**Fig. 3A**).
187 Survival of UTI89Δ*miaA* was restored by complementation with pMiaA$_{nat}$. To ensure that
188 reduced survival of UTI89Δ*miaA* was attributable to hypoosmotic stress and not
189 starvation, cells were resuspended in ddH_2O containing 0.1% glucose, which is
190 comparable to the glucose levels within our M9 medium. Viable bacteria measured after
191 120 minutes indicated that the death of UTI89Δ*miaA* was not due to nutrient deprivation
192 (**Fig. 3B**). We also observed that UTI89Δ*miaA* grew poorly in hyperosmotic conditions,
193 created by addition of 5% NaCl to standard LB (**Fig. 3C**). As in other assays, UTI89Δ*miaB*
194 behaved more like the wild-type strain. Growth of UTI89Δ*miaA* was restored to wild-type
195 levels by complementation with pMiaA$_{nat}$ (**Fig. 3D**). These results indicate that the *miaA*
196 knockout has decreased resistance to both hypo- and hyperosmotic stresses.
197
198 ***Hyperosmotic stress attenuates MiaA translation***
199 We next examined how MiaA levels in UTI89 change in response to environmental
200 cues, focusing on hyperosmotic stress. For these assays, we employed a low-copy

number plasmid (pMiaA-Flag$_{nat}$) that encodes C-terminal FLAG-tagged MiaA under control of the native *miaA* promoter. Mid-logarithmic phase cultures of UTI89/pMiaA-Flag$_{nat}$ were resuspended in LB ± 5% NaCl and levels of MiaA-Flag were then assessed by western blot at 30-minute intervals over the course of 1.5 hours (**Fig. 4A**). Interestingly, MiaA levels in UTI89 exposed to high salt broth were decreased at all time points in comparison with bacteria grown in standard LB. We observed a similar phenomenon if overnight cultures of UTI89/pMiaA-Flag$_{nat}$ in standard LB were back-diluted into high salt broth and then grown to mid-logarithmic phase (OD_{600}≈0.5, **Fig. 4B**). Of note, in these assays we observed no loss of the pMiaA-Flag$_{nat}$ construct. In addition, *miaA* transcripts were often elevated following exposure of UTI89 to high salt (**Fig. 4C**), suggesting that the downregulation of MiaA protein levels in response to this osmotic stress occurs via a post-transcriptional mechanism. The transcription of *miaB* was notably reduced under the same conditions (**Fig. 4D**).

To determine if lower amounts of the MiaA protein detected in high salt broth culture affected i^{6}A or ms^{2}i^{6}A levels, we employed liquid chromatography-coupled mass spectrometry (LC-MS). Normalized amounts of the i^{6}A modification in wild-type UT89 grown to mid-logarithmic phase in LB were similar to those measured in UTI89 grown in high salt broth (**Fig. 4E**). However, hyperosmotic stress caused a marked reduction in relative ms^{2}i^{6}A levels (**Fig. 4F**), possibly due to reduced transcription of *miaB* (**Fig. 4D**). i^{6}A and ms^{2}i^{6}A were undetectable in UTI89Δ*miaA*, regardless of high salt exposure, confirming that MiaA is required for both modifications (**Fig. 4E-F**). In contrast, deletion of *miaB* prevented formation of ms^{2}i^{6}A, but led to greatly elevated levels of i^{6}A (**Supplemental Fig. S4**). Cumulatively, these data indicate that in response to

hyperosmotic stress UTI89 can post-transcriptionally downregulate MiaA, coordinate with reduction of both *miaB* messages and ms^2i^6A levels.

Overexpression of MiaA is detrimental under stressful conditions.

Since it was unexpected that high salt stress would lead to a decrease in the levels of MiaA and the ms^2i^6A modification, we set out to determine if overexpression of MiaA would affect bacterial growth during environmental stress. To overexpress MiaA, we utilized a plasmid (pRR48) with *miaA* under control of an IPTG-inducible P*tac* promoter in wild-type UTI89. By LC-MS, relative intensities of i^6A were significantly higher in UTI89/pMiaA$_{Ptac}$ induced with 1 mM IPTG and grown to mid-logarithmic phase in LB compared to UTI89 carrying the empty vector pRR48, whereas the relative intensities of ms^2i^6A were only modestly elevated (**Fig. 5A**).

Next, overnight cultures of UTI89/pMiaA$_{Ptac}$ were back-diluted into LB, LB + 1 mM MV, LB + 5% NaCl, MES-LB, or MES-LB + 1 mM ASN, and grown in the presence of increasing IPTG concentrations (**Fig. 5B-F)**. Lower levels of MiaA protein induction caused no overt defects and the bacteria grew much like UTI89/pRR48. However, higher levels of IPTG-induced MiaA expression hindered growth of UTI89/pMiaA$_{Ptac}$ in the presence of 1 mM MV, 5% NaCl, MES-LB, and 1 mM ASN. In contrast, over expression of MiaB did not affect bacteria growth in these *in vitro* assays (**Supplemental Fig. S5**). These findings indicate that too much MiaA can be detrimental to bacterial fitness, similar to the complete absence of the enzyme.

Both Deletion and Overexpression of MiaA Increase Frameshifting

Previous research in K-12 *E. coli* and *Salmonella* showed that deletion of *miaA* can compromise translational fidelity, resulting in increased ribosomal frameshifting [73, 74]. To determine the effects of MiaA on frameshifting in UTI89, we utilized dual-luciferase reporter plasmids that consist of a translational fusion of firefly luciferase downstream of renilla luciferase. Linker sequences, derived from either Antizyme 1 (Az1) or HIV *gag-pol*, were placed between the two luciferase genes (**Fig. 6A**). The Az1-derived linker sequence contains a stop codon positioned in-frame so that a +1 frameshift must occur for read-through expression of firefly luciferase [75]. In contrast, a -1 frameshift is required for expression of firefly luciferase downstream of the HIV-derived linker [76]. Importantly, upstream of the in-frame stop codons in both linkers are UNN codons that can be recognized by MiaA-modified tRNAs. The firefly and renilla luciferases act on distinct substrates, which are used to sequentially assess levels of expression of each enzyme [75, 76]. Control plasmids in which the two luciferases are in-frame were used to normalize the data by accounting for ribosome drop-off.

To examine the consequences of MiaA expression on frameshifting, the dual-luciferase reporter constructs were used in combination with wild-type UTI89, UTI89Δ*miaA*, UTI89/pMiaA$_{P\mathit{tac}}$, and UTI89 carrying the empty control vector pRR48. After overnight growth in LB, UTI89 and UTI89Δ*miaA* were back-diluted into LB while UTI89/pMiaA$_{P\mathit{tac}}$ and UTI89/pRR48 were back-diluted into LB + 1 mM IPTG to induce MiaA expession. After reaching mid-log growth, the enzymatic activities of the two luciferases were quantified. Both the lack of MiaA and MiaA overexpression caused notable increases in frameshifting in both the +1 and -1 directions (**Fig. 6B-C**). These

results confirm that loss of MiaA can increase frameshifting and show that elevated MiaA levels can likewise impact the fidelity of translation.

Changing levels of MiaA alters the spectrum of expressed proteins

To determine how deletion and overexpression of MiaA affect translation we used multidimensional protein identification technology (MudPIT; LC-MS/MS) with wild-type UTI89 and UTI89Δ*miaA* cultures grown to mid-log phase in LB, and UTI89/pMiaA$_{Ptac}$ and UTI89/pRR48 similarly grown in LB + 1mM IPTG. Of 1,524 proteins detected in UTI89 and UTI89Δ*miaA*, 105 were picked up only in the wild-type strain and 23 were unique to the *miaA* knockout mutant (**Fig. 7A**). 1,471 proteins were identified in UTI89/pRR48 and UTI89/pMiaA$_{Ptac}$, with 42 being exclusive to UTI89/pRR48 and 20 seen only in the MiaA overexpression strain (**Fig. 7B**). 115 proteins were significantly downregulated in UTI89Δ*miaA* relative to wild-type UTI89, while 34 proteins were upregulated in the knockout mutant (**Fig. 7C**). Notably fewer proteins were significantly altered when MiaA was overexpressed. Relative to the control strain UTI89/pRR48, 20 proteins were downregulated in UTI89/pMiaA$_{Ptac}$, whereas nine (including MiaA) were upregulated (**Fig. 7D**).

The specific proteins detected, including those that were differentially expressed due to *miaA* deletion or overexpression, are detailed in **Supplemental Dataset S1**. The differentially expressed proteins were assigned to one or more of 14 functional categories (see *Categories* worksheet and embedded graph in **Supplemental Dataset S1**). A majority of the altered proteins were linked with metabolic pathways, secondary metabolites, and functions associated with the bacterial envelope. These included several

proteins involved in sugar and fatty acid metabolism and the biosynthesis and regulation of electron transport chains (e.g. UbiC, WrbA, ChrR, Qor, NuoM, NudJ, and CyoC). The dysregulation of these factors likely contributed to the various phenotypic defects observed in our *in vitro* and *in vivo* assays and suggested MiaA involvement in other important processes.

In particular, many of the differentially expressed proteins were shown in previous studies to directly or indirectly affect motility or biofilm development. The former group comprised the chemotaxis protein CheA and the flagella-associated proteins FliF, FlhA, and FlgH. Not unexpectedly, both deletion of the *miaA* gene and MiaA overexpression markedly decreased UTI89 motility on swim plates (**Supplemental Fig. S6**). MiaB did not affect motility in these assays. Factors linked with biofilm development include YoaB, the type 1 pilus-associated regulator FimB and periplasmic chaperone FimC, the acid stress-response chaperone HdeB, the cellulose synthase catalytic subunit BcsA, and the cytochrome *bo* subunit CyoC. Using yeast extract-casamino acids (YESCA) medium, which promotes the development of elaborate rugose-colony biofilms [77, 78], we found that UTI89Δ*miaA*, but not UTI89Δ*miaB*, formed atypical biofilms with notably less rugosity than the parent strain (**Fig. 8**). Interestingly, the biofilms formed by UTI89Δ*miaA* were architecturally similar to those formed by a UTI89 mutant lacking the CyoC-interacting partners CyoAB [78].

Our MudPIT results also indicated that MiaA can regulate numerous proteins that have been associated with redox and bacterial responses to nitrosative, oxidative, and more generally, genotoxic stresses (**Supplemental Dataset S1**). Aberrant expression of these factors, including proteins like GadB, CadA, Dps, glutathione S-transferase Gst,

315 and the glutatredoxins GrxB and GrxC, may account for increased sensitivity to oxygen
316 and nitrogen radicals (see **Fig. 2D-H** and **Fig. 5D and F**). Some of these factors, and
317 others like HdeA and HdeB, can also guard against acid stress. Accordingly, follow-up
318 experiments confirmed that UTI89Δ*miaA*, but not UTI89Δ*miaB*, is notably less resistant
319 to acid stress than the wild-type strain (**Supplemental Fig. S7**). On average, relative to
320 wild-type UTI89, UTI89Δ*miaA* titers were reduced over 6,000-fold following exposure to
321 acidic conditions in LB.

322 The sensitivity of both UTI89Δ*miaA* and UTI89/pMiaA$_{P_{tac}}$ to osmotic stress may
323 arise due to the significant downregulation of proteins like SLP, BetB, YggT, ProP, and
324 YnaI (**Supplemental Dataset S1**). Other differentially expressed proteins that probably
325 contribute to the varied phenotypes associated with *miaA* deletion or MiaA
326 overexpression in our assays include multiple transcriptional regulators, several
327 ribosome- and RNA-associated factors, and the tRNA ligases LysU, TyrS, and PheS.
328 These findings indicate that MiaA is tied into a complex web of factors that can have direct
329 and indirect effects on translation. Driving this point home is the observation that MiaA
330 overexpression suppresses the production of TadA, an enzyme that catalyzes the
331 deamination of adenosine-to-inosine (A-to-I) in Arg2 tRNA and a select set of mRNAs
332 [79, 80]. In K-12 *E. coli,* the A-to-I editing function of TadA can recode at least 12 mRNAs,
333 which results in the generation of proteins with altered activities that can impact bacterial
334 cell physiology [80]. Among the known TadA-edited transcripts is one encoding IlvC, an
335 enzyme involved in isoleucine and valine biosynthesis which, like TadA, is downregulated
336 ~3.5-fold in UTI89 when MiaA is overexpressed (**Fig. 7D**).
337

338 ***UTI89ΔmiaA phenotypes are not entirely due to aberrant RpoS or Hfq expression***

339 In K-12 *E. coli*, the deletion of *miaA* results in decreased translation of the alternate
340 Sigma factor RpoS (σ^S) and the small RNA chaperone Hfq [7, 30, 31]. Both of these
341 factors are important for the stress resistance and virulence potential of ExPEC [62, 81].
342 In line with results from K-12 *E. coli*, our proteomics analysis indicated that RpoS and Hfq
343 levels were reduced 2.5- and 2.8-fold, respectively, in UTI89Δ*miaA* relative to the wild-
344 type strain (**Fig. 7C** and **Supplemental Dataset S1**). RpoS downregulation in the
345 absence of *miaA* was also confirmed by western blot analysis (**Supplemental Fig. S8A**)
346 These observations suggest that the phenotypic defects associated with UTI89Δ*miaA*
347 might be attributable to aberrant expression of RpoS or Hfq. However, despite some
348 similarities, the phenotypes that we previously observed with UTI89 mutants lacking
349 either *rpoS* or *hfq* are distinct from one another and from those that we report here with
350 UTI89Δ*miaA* [62, 81]. Furthermore, the induced expression of recombinant RpoS or Hfq
351 (**Supplemental Fig. S8B and C)** failed to rescue growth of UTI89Δ*miaA* under
352 hyperosmotic conditions (**Supplemental Fig. S8D and E**). The pRpoS$_{Ptac}$ and pHfq$_{Ptac}$
353 expression constructs used in these assays can complement UTI89 mutants lacking *rpoS*
354 or *hfq*, respectively [62, 81]. Cumulatively, these data indicate that the phenotypes seen
355 with UTI89Δ*miaA* are not entirely due to attenuated expression of either RpoS or Hfq.
356 Also of note, our ability to complement UTI89Δ*miaA* with MiaA expression constructs (see
357 **Figs. 2, 3,** and **8**) demonstrates that the phenotypic defects associated with this knockout
358 mutant are not caused by off target mutations or polar effects on *hfq*, which lies
359 immediately downstream of *miaA*.
360

361 ***UNN-Leu codon usage by MiaA-sensitive transcripts***

362 Messages like those encoded by *rpoS* and *hfq* are classified as Modification
363 Tunable Transcripts (MoTTs), which are identifiable by 1) codon usage different from that
364 of average transcripts and 2) translation that is sensitive to changing levels of tRNA
365 modifications [31, 82]. Studies in the K-12 *E. coli* strain MG1655 of *rpoS*, *hfq*, and other
366 transcripts suggest that MiaA-sensitive MoTTs have higher than average ratios of UNN-
367 Leu codons relative to total Leu codons [30, 31]. This led us to ask if UNN-Leu codon
368 usage correlates with protein expression levels in UTI89 when MiaA is either absent or
369 over-produced. Plotting results from our MudPIT analysis versus UNN-Leu codon usage
370 (**Supplemental Dataset S1**) showed that just over 60% of the proteins that are
371 differentially expressed in UTI89Δ*miaA* or UTI89/pMiaA$_{P\mathit{tac}}$ have UNN-Leu codon usage
372 ratios that are greater than the K-12 average ratio of 0.22 (**Fig. 9**, green dashed line). In
373 line with previous findings [30, 31], RpoS and Hfq are among the differentially expressed
374 proteins with UNN-Leu codon usage ratios of greater than 0.22. However, the average
375 UNN-Leu codon usage ratio in UTI89 is somewhat higher than that in K-12 *E. coli*. Using
376 this value, which is 0.28, less than half of the proteins that are differentially regulated in
377 UTI89Δ*miaA* or UTI89/pMiaA$_{P\mathit{tac}}$ have greater than average UNN-Leu codon usage ratios
378 (**Fig. 9**, black dashed line). Furthermore, among the proteins that are not significantly
379 altered by either deletion or overexpression of *miaA*, about 30% have UNN-Leu codon
380 usage ratios greater than 0.28. Cumulatively, these data indicate that UNN-Leu codon
381 ratios alone may not be especially useful for predicting MiaA-sensitive protein expression
382 patterns within ExPEC strains like UTI89.
383

DISCUSSION

The results presented here demonstrate that MiaA is crucial for ExPEC fitness and virulence, and that changing MiaA levels can impact the translation of a broad spectrum of proteins. Our findings are in line with previously published work showing that tRNA modifying enzymes can influence the virulence potential of a variety of microbial pathogens [83]. The attenuation of bacterial virulence-related phenotypes in the absence of a specific tRNA modifying enzyme can, in some cases, be explained by sub-optimal translation of specific toxins or key regulatory factors [14, 19-21]. For example, deletion of *miaA* in the diarrheagenic bacteria *Shigella flexneri* ablates translation of the transcriptional master regulator VirF, resulting in the reduced expression of downstream virulence factors [11, 84]. Overexpression of recombinant VirF alone is sufficient to rescue the *miaA* mutant, suggesting that low-level production of VirF is in large part responsible for the virulence-related defects caused by the deletion of *miaA* in *S. flexneri*. In contrast, our work indicates that the diverse phenotypes affected by MiaA expression in the ExPEC isolate UTI89 are not attributable to any single factor, but rather arise due to the altered expression and dysregulation of multiple proteins and pathways downstream of MiaA.

The ms^2i^6A modification is understood to affect the fidelity of translation [5, 8, 27]. Earlier work in K-12 *E. coli* and *Salmonella* strains showed that bacteria lacking *miaA* have an increase in the +1 direction of frameshifting, but not the -1 direction [73, 74]. In these studies, the i^6A modification was found to be a major contributor to ribosome fidelity. In UTI89, significant increases in frameshifting were seen in both the +1 and -1 directions when *miaA* was knocked out. When MiaA was overproduced, we also observed marked elevation of frameshifting in the -1 direction, while frameshifting levels in the +1 direction

were more modest. Most reports to date indicate that tRNA modifications typically affect frameshifting primarily in one direction [5, 74]. At first glance, our data seemingly counter this trend. However, we note that the expression of firefly luciferase downstream of the HIV-derived linker in our reporter system may also occur as a consequence of a +2 frameshift, rather than a -1 frameshift, which would more closely mirror what was observed in previous studies with K-12 *E. coli* and *Salmonella* strains [73, 74]. It is also possible that the apparent increases in both -1 and +1 frameshifting observed in our assays reflect the presence of MiaA-sensitive regulatory circuits in UTI89 that are different from those in K-12 *E. coli* or *Salmonella* strains.

During the course of this study, we were surprised to observe that MiaA levels in the ExPEC reference strain UTI89 were substantially decreased in response to high salt (see **Fig. 4**). Ongoing work indicates that MiaA levels in UTI89 are also altered upon exposure to other stressors, such as MV (**Supplemental Fig. S9A and B**). Due to the sweeping phenotypes seen in the absence of MiaA, we hypothesized that the levels of MiaA would have stayed the same or increased in response to stressors like high salt and MV. However, our data indicate that MiaA levels are fine-tuned within ExPEC such that too much or too little enzyme can have similarly detrimental consequences. The effects of MiaA expression in our growth curve assays were dose–dependent, with high-level expression of MiaA being nearly as disruptive as the deletion of *miaA*. For instance, low-level expression of MiaA restored the resistance of UTI89Δ*miaA* to high salt, whereas overexpression of MiaA resulted in greatly increased sensitivity (see **Fig. 5**).

MiaA is part of a complex superoperon and its regulation, and the regulation of tRNA modifying enzymes in general, is not well understood [33, 85, 86]. Though we did

not investigate MiaA regulation in detail here, our RT-qPCR experiments indicate that MiaA levels are reduced in response to high salt stress via a post-transcriptional mechanism (**Fig. 4C**). Interestingly, *miaA* has a higher-than-average UNN Leu codon usage ratio of 0.46, suggesting that MiaA may help regulate the translation of its own transcripts [31]. Furthermore, we note that MiaA levels are intensified in the presence of the metal chelator EDTA (**Supplemental Fig. S9C**), raising the possibility that the quantities of this tRNA modifying enzymes are controlled by one or more EDTA-sensitive metalloproteases. The factors that modulate MiaA levels during times of stress require further investigation.

By adjusting the levels of tRNA modifying enzymes like MiaA, ExPEC and other organisms may be able to vary the diversity of translated proteins and thereby optimize adaptive responses to stressful stimuli [14, 33, 46, 87-90]. Indeed, the overexpression and deletion of *miaA* led to the generation of distinct proteomes by UTI89 (**Fig. 7**) and compromised the ability of this ExPEC strain to deal with multiple stressors. Because tRNA modifications can have pleiotropic effects, it is not always easy to distinguish the direct and indirect effects that tRNA modifying enzymes like MiaA have on translation [90]. For example, pioneering work in K-12 *E. coli* indicates that the efficient translation of RpoS and Hfq relies on MiaA for proper decoding of UNN-Leu codons [7, 30, 31], but these factors can themselves regulate the expression of numerous other proteins [91-93]. The capacity for MiaA to have additional, indirect effects on the fidelity and specificity of translation is further highlighted by our proteomics data showing that MiaA impacts the expression of multiple ribosome- and RNA-associated factors, tRNA ligases, and the RNA editing enzyme YfhC (TadA). These findings suggest the existence of a complex network

of RNA and translational modifiers that can regulate the expression of one another. Layered on top of this is the potential for MiaA to affect the biosynthesis and availability of specific metabolites used by other tRNA modifying enzymes [15, 33].

Increases in frameshifting due to changing levels of MiaA may also allow for more error-prone translation and the subsequent diversification of expressed proteins, which could allow bacteria to better deal with stressful stimuli. The ability of cells to actively regulate frameshifting and other translational errors in order to generate mutant proteins that deviate from those encoded by the genome is gaining appreciation as an adaptive response to stress [94-97]. Ongoing studies aim to utilize ribosomal profiling along with RNA-seq and proteomics to determine if off-frame and mutant proteins are being produced by ExPEC via translational modifiers like MiaA in response to stressful stimuli. Similar lines of research may also shed light on the somewhat more cryptic functions of the MiaB-catalyzed tRNA modification.

In the absence of *miaA*, the i^6A and ms^2i^6A modifications are not detectable (**Fig. 4**), as expected from previously published work [86]. When MiaA is overproduced, high levels of i^6A are observed, while ms^2i^6A modification levels remain relatively stable (**Fig. 5A**). This suggests that only a fraction of the UNN-decoding tRNAs are fully modified in the cell at any time. Interestingly, high salt stress reduces both MiaA expression and ms^2i^6A levels, but does not significantly affect i^6A levels (**Fig. 4**). In contrast, the disruption of *miaB* prevents the formation of ms^2i^6A and causes marked increases in i^6A levels (**Supplemental Fig. S4**), but this had no phenotypic effect in any of our assays. These findings present a conundrum – why does high-level production of i^6A due to MiaA overexpression attenuate the stress resistance of UTI89 while even higher levels of i^6A

that build up in the absence of MiaB had no overt phenotypic effects in our assays? In considering this issue, it should be noted that we quantified relative levels of i^6A and ms^2i^6A, and not specific tRNAs, leaving open the possibility that changing levels of MiaA differentially affect distinct tRNA subsets. This alone could account for the contrasting phenotypic effects linked with elevated i^6A levels due to MiaA overexpression versus those caused by *miaB* deletion. MiaA overexpression may also be detrimental due to depletion of substrates like dimethylallyl diphosphate (DMAPP) that feed into other critical pathways, including the biosynthesis of ubiquinone. The deletion of *miaB*, by causing a buildup of i^6A rather than accelerated production of this modified residue, may have less of an abrupt impact on the availability substrates like DMAPP. Finally, it is feasible that MiaA has moonlighting function(s), affecting non-tRNA targets and compromising bacterial fitness when produced in excess. Cumulatively, the findings presented here highlight the central and complex roles that core metabolic genes like *miaA* can have on the elaboration and fine-tuning of pathogen stress resistance and virulence-associated phenotypes.

EXPERIMENTAL PROCEDURES

Bacterial strains. Strains used in this study are listed in **Supplemental Table S1**. Mutant strains were constructed in the reference ExPEC isolate UTI89 using the lambda Red recombination system and primers detailed in **Supplemental Table S2**, as previously described [48]. The chloramphenicol resistance (Clm^R) cassette flanked by LoxP sites was amplified from plasmid pKD3 using primers that contain overhanging ends with ~40 bp of homology near the 5' and 3' ends of each target locus. PCR products were

499 introduced by electroporation into UTI89 carrying pKM208, which encodes an IPTG-
500 inducible lambda Red recombinase [49]. Knockouts were verified by PCR using primers
501 indicated in **Supplemental Table S2**.
502
503 ***Plasmids***. Expression and reporter constructs were generated using standard molecular
504 biology approaches and primers listed in **Supplemental Table S2**. The *miaA* and *miaB*
505 genes were amplified from UTI89 by PCR, digested, and ligated into pRR48 using Pst1
506 and Kpn1 restriction sites to create pMiaA$_{P\mathit{tac}}$ and pMiaB$_{P\mathit{tac}}$. Sequences encoding Hfq
507 fused with C-terminal 6xHis and Flag tags were cloned using a similar approach to make
508 pHfq$_{P\mathit{tac}}$. To create pMiaA$_{nat}$, the UTI89 *miaA* sequence was amplified along with 200
509 base pairs of flanking sequences, including the *miaA* promoter, and then ligated into the
510 EcoR1 site of pACYC184. The plasmid pMiaA-Flag$_{nat}$, having the *miaA* promoter region
511 upstream of sequences encoding MiaA with a C-terminal Flag-tag, was produced
512 similarly.
513 The dual-luciferase reporter plasmids used for the frameshifting assays were
514 created using p2Luc plasmids as templates [75, 76]. The genes encoding the renilla and
515 firefly luciferases were amplified by PCR along with intergenic Az1- or HIV-derived linker
516 sequences. A Shine-Dalgarno ribosome binding site was incorporated into the forward
517 primer (p2Luc_F) primer to promote translation of the linked luciferases. PCR products
518 were digested and ligated into the KpnI and HindIII sites of pBAD18 (Ap^R) and pBAD33
519 (Cam^R). Plasmids with different resistance cassettes were needed for use with
520 UTI89Δ*miaA* (Cam^R) and UTI89 carrying pMiaA$_{P\mathit{tac}}$ or the empty vector pRR48. The Az1-
521 and HIV-derived linker region sequences are noted in **Fig. 6A**, and were chosen because

522 they contain MiaA-sensitive UNN codons. Control plasmids in which the Az1 and HIV
523 linkers are altered to place the two luciferases in-frame were generated in an analogous
524 fashion using previously described p2Luc plasmids as templates [75, 76].
525
526 ***Bacterial growth analysis.*** UTI89 and its derivatives were grown from frozen stocks in
527 5 ml of LB, 100 mM MES-buffered LB (MES-LB; pH 5.0), or modified M9 medium (6 g/liter
528 Na_2HPO_4, 3 g/l KH_2PO_4, 1 g/l NH_4Cl, 0.5 g/l NaCl, 1 mM $MgSO_4$, 0.1 mM $CaCl_2$, 0.1%
529 glucose, 0.0025% nicotinic acid, 0.2% casein amino acids, and 16.5 μg/ml thiamine in
530 H_2O) at 37°C overnight in loosely capped 20-by-150-mm borosilicate glass tubes with
531 shaking (225 rpm, with tubes tilted at a 30° angle). Overnight cultures were brought to an
532 OD_{600} of ~1.0 and then sub-cultured 1:100 into LB, MES-LB, or M9 medium. Growth
533 curves were acquired using a Bioscreen C instrument (Growth Curves USA) with 200-μl
534 cultures in 100-well honeycomb plates shaking at 37°C. Cultures included extra NaCl (5%
535 w/v), 1 mM MV (Sigma-Aldrich), 1 or 2 mM ASN (Sigma-Aldrich), or IPTG, as indicated.
536 MV and ASN solutions were prepared fresh just before use. All growth curves were
537 determined using quadruplicate samples with at least three independent replicates.
538 Overnight cultures of strains carrying plasmids for complementation experiments were
539 grown in the presence of antibiotics (100 μg of ampicillin/ml or 50 μg of tetracycline/ml)
540 to maintain the plasmids, but antibiotics were not included in media used for the
541 subsequent growth assays.
542
543 ***Mouse models.*** All animals used in this study were handled in accordance with protocols
544 approved by the Institutional Animal Care and Use Committee at the University of Utah

(Protocol number 10-02014), following US federal guidelines indicated by the Office of Laboratory Animal Welfare (OLAW) and described in the Guide for the Care and Use of Laboratory Animals, 8th Edition. Mice were purchased from The Jackson Laboratory, housed 3 to 5 per cage, and allowed to eat (irradiated Teklad Global Soy Protein-Free Extruded chow) and drink antibiotic-free water *ad libitum*.

Competitive gut colonization assays. For these assays, a kanamycin resistance cassette (Kan^R) was inserted into the *att*Tn7 site of UTI89 to create UTI89::Kan^R, which can be easily distinguished from the chloramphenicol resistant (Cam^R) *miaA* and *miaB* knockout mutants by plating on selective media. Previous work demonstrated that insertion of resistance cassettes into the *att*Tn7 site does not impact ExPEC fitness within the gut [55, 56]. Individual cultures of UTI89::Kan^R (standing in as the wild-type strain), UTI89Δ*miaA*, and UTI89Δ*miaB* were grown statically from frozen stocks for 24 h at 37°C in 250-ml flasks containing 20 ml of modified M9 medium. Each knockout mutant was then mixed 1:1 with UTI89::Kan^R (6 ml of each culture) and then pelleted by centrifugation at 8,000 x *g* for 8 minutes at room temperature. The bacterial pellets were then washed once with phosphate-buffered saline (PBS), pelleted again, and resuspended in 0.5 ml of PBS. Female SPF BALB/c mice aged 7 to 8 weeks were inoculated via oral gavage with 50 µl PBS containing ~10^9 CFU of each bacterial mixture. At the indicated time points post-inoculation, individual mice were placed into unused takeout boxes for a few minutes for weighing and feces collection. Freshly deposited feces were collected from the boxes and immediately added to 1 ml of 0.7% NaCl, weighed, and set on ice. The samples were then homogenized and briefly centrifuged at low speed to pellet any insoluble debris. Supernatants were serially diluted and plated onto LB agar containing either

chloramphenicol (20 µg/ml) or kanamycin (50 µg/ml) for selective growth of UTI89::Kan^R (wild type), UTI89Δ*miaA*, or UTI89Δ*miaB*. Fecal samples were also analyzed prior to the start of each experiment to ensure that there were no endogenous bacteria present that were resistant to chloramphenicol or kanamycin. CIs were calculated as the ratio of knockout over wild-type bacteria recovered in the feces divided by the ratio of knockout over wild-type bacteria present in the inoculum [55, 57]. A total of 7 to 8 mice in two independent assays were used for each set of bacterial strains tested.

UTI model. The murine UTI model was used essentially as described by our group and others [98, 99]. Wild-type UTI89 and the *miaA*, and *miaB* knockout mutants were grown from frozen stocks in 20 ml LB broth in 250 mL Erlenmeyer flasks without shaking at 37°C for 24 hours. Bacteria were then pelleted by centrifugation (8 minutes at 8,000 x g) and resuspended in PBS. Seven- to eight-week-old female CBA/J or C3H/HeJ mice were briefly anesthetized by isoflurane inhalation and slowly inoculated via transurethral catheterization with 50 µL of PBS containing a suspension of ~10^7 bacteria. Bacterial reflux into the kidneys using this procedure is rare, occurring in less than 1% of the test animals. At 0.25, 1, 3, or 9 days post-inoculation, mice were sacrificed and bladders were harvested aseptically, weighed, and homogenized in 1 ml PBS containing 0.025% Triton X-100. Bacterial titers within the homogenates were determined by plating serial dilutions on LB agar plates. Nine or more mice in total, from two independent experiments, were used for each bacterial strain and time point examined.

Sepsis model. UTI89, UTI89Δ*miaA*, and UTI89Δ*miaB* were grown from frozen stocks in 20 ml M9 broth without shaking at 37°C for 24 h, pelleted by centrifugation at 8,000 x *g* for 8 minutes, and washed once with PBS, pelleted again, and resuspended in

PBS. Seven- to eight-week-old female C57Bl/6 mice were briefly anesthetized by isoflurane inhalation and infected via intraperitoneal injection of ~10^7 CFU within 200 μl PBS. Mice were monitored over a 72-hour period for signs of morbidity and mortality. Alternatively, at 6 hours post-inoculation mice were sacrificed and the liver, kidneys, and spleens were harvested aseptically, weighed, and homogenized in 1 ml PBS containing 0.025% Triton X-100. Bacterial titers within the homogenates were determined by plating serial dilutions on LB agar plates.

Invasion, adhesion, and intracellular persistence assays. Bacteria were grown at 37°C for 48 h in 20 mL static LB broth to induce expression of type 1 pili, which are important mediators of UPEC adherence and entry into host cells [99]. Host cell association and gentamicin protection-based invasion and overnight intracellular persistence assays were performed as previously described using the human bladder epithelial cell line 5637 (HTB-9; ATCC) [100]. Of note, UTI89Δ*miaA* is about 3-fold more sensitive to the host-cell impermeable antibiotic gentamicin, as determined by using Etest Strips (VWR) (**Supplemental Fig. S10**). However, this likely had no effect on results from the cell culture-based invasion and intracellular survival experiments, as the concentrations of gentamicin (100 and 10 μg/ml) used in these assays exceed those needed to effectively kill extracellular UTI89, UTI89Δ*miaB*, and UTI89Δ*miaA*.

Biofilm analysis. *In vitro* rugose biofilm assays were performed starting with cultures grown overnight at 37°C shaking in LB, as described [78]. Bacteria from each culture were then brought to an OD_{600} of ~1.0 and 10 μl aliquots were spotted onto YESCA agar

614 plates (12 g/l Casamino acids, 1.2 g yeast extract, 22 g agar) and incubated at RT (~20-
615 22˚C). After 14 days, biofilm images were acquired by focus stacking using an M.Zuiko
616 Digital ED 60 mm lens mounted on an Olympus OM-D E-M1 Mark II camera.
617
618 ***Motility assays.*** Cultures of UTI89, UTI89Δ*miaA*, and UTI89Δ*miaB* grown overnight
619 shaking in LB or M9 medium were brought to OD_{600} of 1.0. Swim motility plates, containing
620 0.2% agar in LB or M9 medium, were inoculated with 2 µl of each bacterial suspension
621 delivered just below the agar surface. The diameter of bacterial spreading was measured
622 every 1-2 hours over the course of an 8-10 hour-incubation at 37ºC. Swim rates were
623 calculated during logarithmic growth. To assess the effects of MiaA and MiaB
624 overexpression on motility, tryptone soft agar plates [101] containing 50 µg/ml ampicillin
625 and 100 µM IPTG were inoculated with UTI89/pRR48, UTI89/pMiaA$_{Ptac}$, and
626 UTI89/pMiaB$_{Ptac}$ from overnight shaking cultures. Plates were imaged after a 6-hour
627 incubation at 37ºC.
628
629 ***Acid resistance assays.*** Bacterial strains from overnight cultures were diluted 1:100 in
630 fresh LB and grown shaking at 37°C for 3 h. Concentrated HCl was then added to each
631 culture to adjust the pH to 3.0 and incubations were continued for another 30 minutes.
632 Bacteria from 1 ml of each culture were then pelleted at 16,000 x *g* for 5 min and washed
633 in PBS. Surviving bacteria were enumerated by plating serial dilutions on LB agar and
634 normalized to input titers.
635

636 ***Osmotic stress resistance assays.*** UTI89/pACYC184, UTI89Δ*miaA*/pACYC184,
637 UTI89Δ*miaA*/pMiaA$_{nat}$, and UTI89Δ*miaB* were grown shaking overnight at 37°C in 5 ml
638 LB broth with 20 µg/ml tetracycline and then back diluted 1:100 into 5 ml fresh LB (+
639 tetracycline). After 5 h shaking at 37°C, a 1-ml aliquot of each culture was pelleted,
640 resuspended in 1 ml of sterile water with or without 0.1% glucose, and incubations were
641 continued for another 2 h with shaking at 37°C. Viable bacteria present at 0, 30, 60, 90,
642 and 120 min after resuspension in water were quantified by dilution plating and
643 normalized to input titers. Growth curves in LB ± 5% NaCl were acquired as described
644 above.
645
646 ***Western blot analysis.*** Bacterial pellets were frozen at -80˚C and then resuspended in
647 B-PER lysis reagent (Thermo Scientific) supplemented with 1 mM phenylmethylsulfonyl
648 fluoride, protease inhibitor cocktail (Roche), and Lysonase Bioprocessing Reagent
649 (Novagen). After a 15-minute incubation at room temperature, samples were spun for 1
650 minute at 13,000 x *g* to remove large cell debris, and protein concentrations in the
651 supernatants were determined using the BCA reagent system (Pierce). Equivalent protein
652 amounts were resolved by SDS-PAGE and subsequently transferred to Immobilon PVDF-
653 FL membranes (Millipore). Blots were probed using mouse anti-Flag M2 (1:3000; Sigma-
654 Aldrich), rabbit anti-Flag (Immunology Consultants laboratory, inc.), and mouse anti-
655 RpoS (anti-SigmaS; Biolegend) and visualized using enhanced chemiluminescence with
656 HRP-conjugated secondary antibodies (1:3000 or 1:5000; Amersham Biosciences), as
657 described [102]. To ensure that equivalent amounts of protein from each sample were
658 analyzed, blots were re-probed using rabbit anti-*E. coli* antisera (1:2,000 or 1:5000;
659 BioDesign International).

Analysis of relative i6A and ms2i6A levels. UTI89 and UTI89Δ*miaA* were grown from frozen stocks shaking at 37˚C overnight in LB. UTI89/pRR48 and UTI89/pMiaA$_{Ptac}$ were grown similarly using LB supplemented with ampicillin (100 μg/ml). The bacteria were sub-cultured 1:100 into 6 ml of LB ± 1 mM IPTG and then grown shaking to an OD_{600} of 0.5. After adjusting the cultures to OD_{600} of 1.0, the bacteria were pelleted by spinning at 8000 x *g* for 1.5 minutes. Pellets were then resuspended in 1 ml of RNA*later* Stabilization Solution (ThermoFisher) and stored at 4˚C overnight prior to extraction of RNA using a Norgen Total RNA Extraction Kit.

Samples were analyzed using a Hypersil GOLD C18 column (2.1 mm × 150 mm, 1.9 μm particle size; Thermo Fisher) attached to a Thermo Scientific Dionex UltiMate 3000 UHPLC instrument in line with an LTQ-OrbiTrap XL instrument (Thermo Fisher). The LC-MS parameters were based upon a procedure described previously [103, 104], with the following adjustments. The UHPLC column was pre-equilibrated in 100% Buffer A [50 mM ammonium acetate (Fisher) in LC–MS Optima water]. Buffer B consisted of 60% (v/v) LC–MS Optima acetonitrile (Fisher) and 40% LC–MS water (Fisher). The reaction components were eluted at a rate of 0.2 ml/minute with the following program: 0% B from 0 to 3.46 min, 0 to 0.9% B from 3.46 to 3.69 min, 0.9 to 1.5% B from 3.69 to 3.92 min, 1.5 to 3% B from 3.92 to 4.25 min, 3 to 20% B from 4.25 to 6.5 min, 20 to 25% B from 6.5 to 7 min, 25 to 40% B from 7 to 8.5 min, 40 to 45% B from 8.5 to 9.25 min, 45 to 60% B from 9.25 to 9.95 min, 60 to 100% B from 9.95 to 10.45 min, 100% B from 10.45 to 16 min, 100 to 0% B from 16 to 16.1 min, and 0% B from 16.1 to 20 min. The

682 flow from the column was diverted to the mass spectrometer from 3.5 minutes to 17
683 minutes during the UHPLC program. The mass spectrometer was operated in positive
684 ion mode, and authentic guanosine material (Sigma Aldrich) was used to generate a
685 tune file for the instrument. The observed *m/z* values of the +1 charge states of the i6a
686 and ms2i6a RNA bases were 336.1658 and 382.1535, respectively. The observed
687 retention times for i6A and ms2i6a were determined from the center of their extracted
688 ion chromatogram peaks to be 15.55 and 16.45 minutes, respectively. The retention
689 time of i6a from biological extracts was consistent with the retention time of authentic
690 i6a material (Cayman Chemical). Absolute intensities of the i6a ions were retrieved from
691 the mass spectrum scanned between 15.4 – 16.1 minutes, while the absolute intensities
692 of the ms2i6a ions were retrieved from the mass spectrum scanned between 16.2 and
693 17.0 minutes. The scan range was chosen to include the entire peak of an EIC trace,
694 excluding mass spectral data recorded out of these bounds. This ensured that the
695 intensities of ions 336.17 and 382.15 arise from eluted i^6A and ms^2i^6A material and did
696 not include background during the rest of the run. The scan windows were wide enough
697 to account for any small drift in retention that might occur from sample to sample.
698 Because total RNA concentration varied by sample, the samples were normalized
699 against the total RNA concentration of each sample, as estimated via a NanoDrop
700 measurements at 260 nm.

701 ***Quantification of frameshifting.*** UTI89, UTI89Δ*miaA,* UTI89/pRR48 and
702 UTI89/pMiaA$_{Ptac}$ carrying one of the dual-luciferase reporter plasmids (see
703 **Supplemental Table S1**) were grown overnight in LB supplemented with
704 chloramphenicol (20 μg/ml) or ampicillin (100 μg/ml). The cells were sub-cultured 1:100

into 6 ml LB with and without 1mM IPTG. At an OD_{600} of 0.2, arabinose (0.2%) was added to all of the cultures to induce expression of the luciferases. Cells were allowed to continue growing until reaching an OD_{600} of 0.5, at which point the cultures were adjusted to an OD_{600} of 1.0 and pelleted by spinning at 8000 x *g* for 1.5 minutes. The pellets were then subjected to one freeze-thaw cycle before being resuspended in Passive Lysis Buffer (Promega; E1910). One scoop of 0.15 mm zirconium oxide beads (Next Advance; ZrOB015) was added to each tube and bacteria were lysed using a Bullet Blender (Next Advance) set at speed 8 for 3 min. After a 30-second spin in a microfuge to pellet beads and any large debris, the supernatants were collected and luciferase activities were analyzed as previously described [76]. Briefly, the Dual-Luciferase Reporter Assay System (Promega) was used in combination with the Veritas Microplate Luminometer from Turner Biosystems to quantify activity of the two luciferases. Frameshifting was calculated by first determining the ratio of firefly to renilla luciferase activity for each sample, and then normalizing each out-of-frame construct (pCWR43 and pCWR45) with their associated in-frame control (pCWR42 and pCWR44, respectively).

Proteomics. UTI89, UTI89Δ*miaA,* UTI89/pRR48, and UTI89/pMiaA$_{P\mathit{tac}}$ were grown to mid-log phase (OD_{600}~0.5) in LB shaking at 37°C. IPTG (1 mM) was included for UTI89/pRR48 and UTI89/pMiaA$_{P\mathit{tac}}$. About 1X10^9 CFU from each culture was pelleted at 8,000 x *g* for 1.5 minutes. Supernatants were then removed and cells were plunged into liquid nitrogen and subsequently analyzed using MudPIT with the MSRC Proteomics Core at Vanderbilt University. Label-free quantification (LFQ) values were loaded into Prostar

728 software for statistical analysis and visualization. The data set was filtered by requiring all
729 conditions to contain at least two values. Imputation for partially observed values was
730 done with the Structured Least Square Adaptative algorithm. Imputation for conditions in
731 which values were missing for a specific protein in all three biological replicates used the
732 DetQuantile algorithm with the settings Quantile:2.5 and Factor:1. Statistical analysis was
733 performed using the 1vs1 settings and Student's *t*-tests. Differentially expressed proteins
734 were categorized (**Supplemental Dataset S1**) based on literature searches and
735 information drawn from EcoCyc ([105]; http://ecocyc.org/), STRING Protein-Protein
736 Interaction Networks Functional Enrichment Analysis ([106]; https://string-db.org/), and
737 Phyre2 ([107]; http://www.sbg.bio.ic.ac.uk/~phyre2/html/page.cgi?id=index). The
738 proteomics output files will be uploaded to ProteomeXchange.
739
740 **RT-qPCR analysis.** UTI89 was diluted 1:100 from overnight cultures into fresh LB, grown
741 shaking for 2.5 hours at 37°C prior to resuspension in LB or LB + 5% NaCl. After another
742 one-hour incubation bacteria were pelleted and total RNA was extracted using the
743 miRNeasy mini kit (QIAGEN). RNA samples were treated with RNase-Free DNase
744 (QIAGEN) and cDNA was made using SuperScript IV VILO Master Mix (Invitrogen)
745 according to the manufacturer's protocol. Quantitative PCR (qPCR) was carried out using
746 primers listed in **Supplemental Table S2** with the PowerUp SYBR Green Master Mix
747 (Thermo Fisher Scientific) on a QuantStudio 3 Real-Time PCR Instrument (Applied
748 Biosystems). Replicas were made for each cDNA sample and *miaA* and *miaB* levels
749 were normalized to *rpoD*. Products were resolved in 1.5% agarose gels, stained with

ethidium bromide, and visualized using a GelDoc system (BioRad Technologies) to help verify the specificity of the RT-qPCR results.

Codon usage analysis. Codon frequencies (UNN Stats tab, **Supplemental Dataset S1**) were calculated for each gene in UTI89 (accessions CP000243.1 and CP000244.1) using custom Python scripts that leverage the BioPython and NumPy packages.

Statistical analysis. *P* values were determined as indicated by Log-Rank (Mantel-Cox), Mann-Whitney U tests, ANOVA, or Student's *t*-tests performed using Prism 9.0.0 software, with corrections as indicated (GraphPad Software). Data distribution normality (Gaussian) was not assumed, such that non-parametric tests were used for the mouse experiments. *P*-values of less than or equal to 0.05 were defined as significant.

ACKNOWLEDGEMENTS

We thank W. Hayes McDonald of the Vanderbilt School of Medicine Mass Spectrometry Research Center for help with the proteomics. This study was funded in part by NIH grants to M.A.M. (GM134331, AI135918, AI095647, and AI088086) and to V.B. (GM126956). M.G.B. was supported by T32 AI055434 from the National Institute of Allergy and Infectious Diseases, and A.J.L. was supported by T32 DK007115 from the National Institute of Diabetes and Digestive and Kidney Diseases. The authors have no conflicts of interest to declare.

Author Contributions

MGB, BAF, and MAM designed, supervised the study, performed research, analyzed the data, and drafted the paper. WMK, AJL, JRB, MH, VB, and MTH helped with design, experimentation, and editing. AT, CJB, LMB, and QZ performed experiments and helped process samples. All authors contributed to and approved the submission of this paper.

REFERENCES

1. Jackman JE, Alfonzo JD. Transfer RNA modifications: nature's combinatorial chemistry playground. Wiley Interdiscip Rev RNA. 2013;4(1):35-48. doi: 10.1002/wrna.1144. PubMed PMID: 23139145; PubMed Central PMCID: PMCPMC3680101.

2. Bjork GR, Durand JM, Hagervall TG, Leipuviene R, Lundgren HK, Nilsson K, et al. Transfer RNA modification: influence on translational frameshifting and metabolism. FEBS Lett. 1999;452(1-2):47-51. Epub 1999/06/22. PubMed PMID: 10376676.

3. Gustilo EM, Vendeix FA, Agris PF. tRNA's modifications bring order to gene expression. Curr Opin Microbiol. 2008;11(2):134-40. doi: 10.1016/j.mib.2008.02.003. PubMed PMID: 18378185; PubMed Central PMCID: PMCPMC2408636.

4. Boccaletto P, Machnicka MA, Purta E, Piatkowski P, Baginski B, Wirecki TK, et al. MODOMICS: a database of RNA modification pathways. 2017 update. Nucleic Acids Research. 2018;46(D1):D303-d7. Epub 2017/11/07. doi: 10.1093/nar/gkx1030. PubMed PMID: 29106616; PubMed Central PMCID: PMCPMC5753262.

5. Bjork GR, Hagervall TG. Transfer RNA Modification: Presence, Synthesis, and Function. EcoSal Plus. 2014;6(1). doi: 10.1128/ecosalplus.ESP-0007-2013. PubMed PMID: 26442937.

6. Blum PH. Reduced leu operon expression in a *miaA* mutant of *Salmonella typhimurium*. J Bacteriol. 1988;170(11):5125-33. Epub 1988/11/01. PubMed PMID: 3141379; PubMed Central PMCID: PMC211580.

7. Thompson KM, Gottesman S. The MiaA tRNA modification enzyme is necessary for robust RpoS expression in *Escherichia coli.* J Bacteriol. 2014;196(4):754-61. doi:

802 10.1128/JB.01013-13. PubMed PMID: 24296670; PubMed Central PMCID:
803 PMCPMC3911166.
804 8. Schweizer U, Bohleber S, Fradejas-Villar N. The modified base
805 isopentenyladenosine and its derivatives in tRNA. RNA biology. 2017;14(9):1197-208.
806 Epub 2017/03/10. doi: 10.1080/15476286.2017.1294309. PubMed PMID: 28277934;
807 PubMed Central PMCID: PMCPMC5699536.
808 9. Ahn KS, Ha U, Jia J, Wu D, Jin S. The truA gene of *Pseudomonas aeruginosa* is
809 required for the expression of type III secretory genes. Microbiology. 2004;150(Pt
810 3):539-47. Epub 2004/03/03. PubMed PMID: 14993303.
811 10. Shippy DC, Fadl AA. tRNA modification enzymes GidA and MnmE: potential role
812 in virulence of bacterial pathogens. Int J Mol Sci. 2014;15(10):18267-80. doi:
813 10.3390/ijms151018267. PubMed PMID: 25310651; PubMed Central PMCID:
814 PMCPMC4227215.
815 11. Durand JM, Dagberg B, Uhlin BE, Bjork GR. Transfer RNA modification,
816 temperature and DNA superhelicity have a common target in the regulatory network of
817 the virulence of *Shigella flexneri*: the expression of the *virF* gene. Mol Microbiol.
818 2000;35(4):924-35. Epub 2000/02/26. PubMed PMID: 10692168.
819 12. Chaudhuri RR, Peters SE, Pleasance SJ, Northen H, Willers C, Paterson GK, et
820 al. Comprehensive identification of *Salmonella enterica* serovar Typhimurium genes
821 required for infection of BALB/c mice. PLoS Pathog. 2009;5(7):e1000529. doi:
822 10.1371/journal.ppat.1000529. PubMed PMID: 19649318; PubMed Central PMCID:
823 PMCPMC2712085.
824 13. Gray J, Wang J, Gelvin SB. Mutation of the *miaA* gene of *Agrobacterium*
825 *tumefaciens* results in reduced vir gene expression. J Bacteriol. 1992;174(4):1086-98.
826 Epub 1992/02/01. PubMed PMID: 1735704; PubMed Central PMCID: PMC206401.
827 14. Chionh YH, McBee M, Babu IR, Hia F, Lin W, Zhao W, et al. tRNA-mediated
828 codon-biased translation in mycobacterial hypoxic persistence. Nature Comm.
829 2016;7:13302. Epub 2016/11/12. doi: 10.1038/ncomms13302. PubMed PMID:
830 27834374; PubMed Central PMCID: PMCPMC5114619.
831 15. Koshla O, Yushchuk O, Ostash I, Dacyuk Y, Myronovskyi M, Jager G, et al.
832 Gene miaA for post-transcriptional modification of tRNAXXA is important for

morphological and metabolic differentiation in Streptomyces. Mol Microbiol. 2019;112(1):249-65. Epub 2019/04/25. doi: 10.1111/mmi.14266. PubMed PMID: 31017319.

16. Thongdee N, Jaroensuk J, Atichartpongkul S, Chittrakanwong J, Chooyoung K, Srimahaeak T, et al. TrmB, a tRNA m7G46 methyltransferase, plays a role in hydrogen peroxide resistance and positively modulates the translation of *katA* and *katB* mRNAs in *Pseudomonas aeruginosa*. Nucleic acids research. 2019;47(17):9271-81. Epub 2019/08/21. doi: 10.1093/nar/gkz702. PubMed PMID: 31428787; PubMed Central PMCID: PMCPMC6755087.

17. Gao T, Tan M, Liu W, Zhang C, Zhang T, Zheng L, et al. GidA, a tRNA Modification Enzyme, Contributes to the Growth, and Virulence of *Streptococcus suis* Serotype 2. Front Cell Infect Microbiol. 2016;6:44. Epub 2016/05/06. doi: 10.3389/fcimb.2016.00044. PubMed PMID: 27148493; PubMed Central PMCID: PMCPMC4835480.

18. Li D, Shibata Y, Takeshita T, Yamashita Y. A novel gene involved in the survival of *Streptococcus mutans* under stress conditions. Applied and Environmental Microbiology. 2014;80(1):97-103. Epub 2013/10/15. doi: 10.1128/AEM.02549-13. PubMed PMID: 24123744; PubMed Central PMCID: PMCPMC3910998.

19. Cho KH, Caparon MG. tRNA modification by GidA/MnmE is necessary for Streptococcus pyogenes virulence: a new strategy to make live attenuated strains. Infection and Immunity. 2008;76(7):3176-86. Epub 2008/04/23. doi: 10.1128/IAI.01721-07. PubMed PMID: 18426891; PubMed Central PMCID: PMCPMC2446735.

20. Kinscherf TG, Willis DK. Global regulation by *gidA* in *Pseudomonas syringae*. J Bacteriol. 2002;184(8):2281-6. Epub 2002/03/27. doi: 10.1128/jb.184.8.2281-2286.2002. PubMed PMID: 11914360; PubMed Central PMCID: PMCPMC134964.

21. Sha J, Kozlova EV, Fadl AA, Olano JP, Houston CW, Peterson JW, et al. Molecular characterization of a glucose-inhibited division gene, *gidA*, that regulates cytotoxic enterotoxin of *Aeromonas hydrophila*. Infection and immunity. 2004;72(2):1084-95. Epub 2004/01/27. doi: 10.1128/iai.72.2.1084-1095.2004. PubMed PMID: 14742556; PubMed Central PMCID: PMCPMC321642.

22. Kaminska KH, Baraniak U, Boniecki M, Nowaczyk K, Czerwoniec A, Bujnicki JM. Structural bioinformatics analysis of enzymes involved in the biosynthesis pathway of the hypermodified nucleoside ms(2)io(6)A37 in tRNA. Proteins. 2008;70(1):1-18. Epub 2007/10/03. doi: 10.1002/prot.21640. PubMed PMID: 17910062.

23. Persson BC. Modification of tRNA as a regulatory device. Mol Microbiol. 1993;8(6):1011-6. Epub 1993/06/01. PubMed PMID: 7689685.

24. Caillet J, Droogmans L. Molecular cloning of the *Escherichia coli miaA* gene involved in the formation of delta 2-isopentenyl adenosine in tRNA. J Bacteriol. 1988;170(9):4147-52. Epub 1988/09/01. PubMed PMID: 3045085; PubMed Central PMCID: PMC211421.

25. Seif E, Hallberg BM. RNA-protein mutually induced fit: structure of *Escherichia coli* isopentenyl-tRNA transferase in complex with tRNA(Phe). J Biol Chem. 2009;284(11):6600-4. Epub 2009/01/23. doi: 10.1074/jbc.C800235200. PubMed PMID: 19158097; PubMed Central PMCID: PMC2652265.

26. Pierrel F, Douki T, Fontecave M, Atta M. MiaB protein is a bifunctional radical-S-adenosylmethionine enzyme involved in thiolation and methylation of tRNA. J Biol Chem. 2004;279(46):47555-63. Epub 2004/09/02. doi: 10.1074/jbc.M408562200. PubMed PMID: 15339930.

27. Ericson JU, Bjork GR. Pleiotropic effects induced by modification deficiency next to the anticodon of tRNA from *Salmonella typhimurium* LT2. J Bacteriol. 1986;166(3):1013-21. Epub 1986/06/01. PubMed PMID: 2423501; PubMed Central PMCID: PMC215226.

28. Eisenberg SP, Yarus M, Soll L. The effect of an *Escherichia coli* regulatory mutation on transfer RNA structure. J Mol Biol. 1979;135(1):111-26. PubMed PMID: 93644.

29. Gowrishankar J, Pittard J. Regulation of phenylalanine biosynthesis in *Escherichia coli* K-12: control of transcription of the *pheA* operon. J Bacteriol. 1982;150(3):1130-7. PubMed PMID: 7042684; PubMed Central PMCID: PMCPMC216333.

30. Aubee JI, Olu M, Thompson KM. TrmL and TusA Are Necessary for *rpoS* and MiaA Is Required for *hfq* Expression in *Escherichia coli*. Biomolecules. 2017;7(2). Epub

2017/05/05. doi: 10.3390/biom7020039. PubMed PMID: 28471404; PubMed Central PMCID: PMCPMC5485728.

31. Aubee JI, Olu M, Thompson KM. The i6A37 tRNA modification is essential for proper decoding of UUX-Leucine codons during *rpoS* and *iraP* translation. RNA (New York, NY). 2016;22(5):729-42. Epub 2016/03/17. doi: 10.1261/rna.053165.115. PubMed PMID: 26979278; PubMed Central PMCID: PMCPMC4836647.

32. Krasich R, Wu SY, Kuo HK, Kreuzer KN. Functions that protect *Escherichia coli* from DNA-protein crosslinks. DNA Repair (Amst). 2015;28:48-59. doi: 10.1016/j.dnarep.2015.01.016. PubMed PMID: 25731940; PubMed Central PMCID: PMCPMC4385401.

33. Connolly DM, Winkler ME. Genetic and physiological relationships among the miaA gene, 2-methylthio-N6-(delta 2-isopentenyl)-adenosine tRNA modification, and spontaneous mutagenesis in *Escherichia coli* K-12. J Bacteriol. 1989;171(6):3233-46. Epub 1989/06/01. PubMed PMID: 2656644; PubMed Central PMCID: PMC210042.

34. Yanofsky C. Mutations affecting tRNATrp and its charging and their effect on regulation of transcription termination at the attenuator of the tryptophan operon. Journal of Molecular Biology. 1977;113(4):663-77. Epub 1977/07/15. PubMed PMID: 330867.

35. Mikkola R, Kurlan CG. Media dependence of translational mutant phenotype. FEMS Microbiol Lett 1988;56(3):265-9. doi: DOI: http://dx.doi.org/10.1111/j.1574-6968.1988.tb03189.x.

36. Forouhar F, Arragain S, Atta M, Gambarelli S, Mouesca JM, Hussain M, et al. Two Fe-S clusters catalyze sulfur insertion by radical-SAM methylthiotransferases. Nat Chem Biol. 2013;9(5):333-8. doi: 10.1038/nchembio.1229. PubMed PMID: 23542644; PubMed Central PMCID: PMCPMC4118475.

37. Leung HC, Chen Y, Winkler ME. Regulation of substrate recognition by the MiaA tRNA prenyltransferase modification enzyme of Escherichia coli K-12. J Biol Chem. 1997;272(20):13073-83. Epub 1997/05/16. PubMed PMID: 9148919.

38. Denamur E, Clermont O, Bonacorsi S, Gordon D. The population genetics of pathogenic *Escherichia coli*. Nat Rev Microbiol. 2021;19(1):37-54. Epub 2020/08/23. doi: 10.1038/s41579-020-0416-x. PubMed PMID: 32826992.

925 39. Vila J, Saez-Lopez E, Johnson JR, Romling U, Dobrindt U, Canton R, et al.
926 *Escherichia coli*: an old friend with new tidings. FEMS microbiology reviews.
927 2016;40(4):437-63. Epub 2017/02/16. doi: 10.1093/femsre/fuw005. PubMed PMID:
928 28201713.
929 40. Barber AE, Norton JP, Spivak AM, Mulvey MA. Urinary tract infections: current
930 and emerging management strategies. Clin Infect Dis. 2013;57(5):719-24. Epub
931 2013/05/07. doi: 10.1093/cid/cit284. PubMed PMID: 23645845; PubMed Central
932 PMCID: PMC3739462.
933 41. Hunstad DA, Justice SS. Intracellular lifestyles and immune evasion strategies of
934 uropathogenic *Escherichia coli*. Annu Rev Microbiol. 2010;64:203-21. Epub 2010/09/10.
935 doi: 10.1146/annurev.micro.112408.134258. PubMed PMID: 20825346.
936 42. Schwab S, Jobin K, Kurts C. Urinary tract infection: recent insight into the
937 evolutionary arms race between uropathogenic *Escherichia coli* and our immune
938 system. Nephrology, Dialysis, Transplantation: official publication of the European
939 Dialysis and Transplant Association - European Renal Association. 2017;32(12):1977-
940 83. Epub 2017/03/25. doi: 10.1093/ndt/gfx022. PubMed PMID: 28340252.
941 43. O'Brien VP, Hannan TJ, Schaeffer AJ, Hultgren SJ. Are you experienced?
942 Understanding bladder innate immunity in the context of recurrent urinary tract infection.
943 Curr Opin Infect Dis. 2015;28(1):97-105. doi: 10.1097/QCO.0000000000000130.
944 PubMed PMID: 25517222; PubMed Central PMCID: PMCPMC4365976.
945 44. Lacerda Mariano L, Ingersoll MA. The immune response to infection in the
946 bladder. Nat Rev Urol. 2020;17(8):439-58. Epub 2020/07/15. doi: 10.1038/s41585-020-
947 0350-8. PubMed PMID: 32661333.
948 45. Svensson L, Poljakovic M, Demirel I, Sahlberg C, Persson K. Host-Derived Nitric
949 Oxide and Its Antibacterial Effects in the Urinary Tract. Adv Microb Physiol. 2018;73:1-
950 62. Epub 2018/09/29. doi: 10.1016/bs.ampbs.2018.05.001. PubMed PMID: 30262107.
951 46. Chan CT, Dyavaiah M, DeMott MS, Taghizadeh K, Dedon PC, Begley TJ. A
952 quantitative systems approach reveals dynamic control of tRNA modifications during
953 cellular stress. PLoS Genet. 2010;6(12):e1001247. Epub 2010/12/29. doi:
954 10.1371/journal.pgen.1001247. PubMed PMID: 21187895; PubMed Central PMCID:
955 PMC3002981.

956 47. Barber AE, Norton JP, Wiles TJ, Mulvey MA. Strengths and Limitations of Model
957 Systems for the Study of Urinary Tract Infections and Related Pathologies. Microbiology
958 and Molecular Biology Reviews: MMBR. 2016;80(2):351-67. Epub 2016/03/05. doi:
959 10.1128/MMBR.00067-15. PubMed PMID: 26935136; PubMed Central PMCID:
960 PMCPMC4867371.
961 48. Datsenko KA, Wanner BL. One-step inactivation of chromosomal genes in
962 *Escherichia coli* K-12 using PCR products. Proc Natl Acad Sci U S A.
963 2000;97(12):6640-5. PubMed PMID: 10829079.
964 49. Murphy KC, Campellone KG. Lambda Red-mediated recombinogenic
965 engineering of enterohemorrhagic and enteropathogenic *E. coli*. BMC Mol Biol.
966 2003;4:11. PubMed PMID: 14672541.
967 50. Forde BM, Roberts LW, Phan MD, Peters KM, Fleming BA, Russell CW, et al.
968 Population dynamics of an *Escherichia coli* ST131 lineage during recurrent urinary tract
969 infection. Nature Comm. 2019;10(1):3643. Epub 2019/08/15. doi: 10.1038/s41467-019-
970 11571-5. PubMed PMID: 31409795; PubMed Central PMCID: PMCPMC6692316.
971 51. Moreno E, Andreu A, Pigrau C, Kuskowski MA, Johnson JR, Prats G.
972 Relationship between *Escherichia coli* strains causing acute cystitis in women and the
973 fecal *E. coli* population of the host. Journal of Clinical Microbiology. 2008;46(8):2529-34.
974 Epub 2008/05/23. doi: 10.1128/jcm.00813-08. PubMed PMID: 18495863; PubMed
975 Central PMCID: PMCPMC2519474.
976 52. Chen SL, Wu M, Henderson JP, Hooton TM, Hibbing ME, Hultgren SJ, et al.
977 Genomic diversity and fitness of *E. coli* strains recovered from the intestinal and urinary
978 tracts of women with recurrent urinary tract infection. Science Translational Medicine.
979 2013;5(184):184ra60. doi: 10.1126/scitranslmed.3005497. PubMed PMID: 23658245;
980 PubMed Central PMCID: PMC3695744.
981 53. Yamamoto S, Tsukamoto T, Terai A, Kurazono H, Takeda Y, Yoshida O. Genetic
982 evidence supporting the fecal-perineal-urethral hypothesis in cystitis caused by
983 *Escherichia coli*. J Urol. 1997;157(3):1127-9. PubMed PMID: 9072556.
984 54. Russo TA, Stapleton A, Wenderoth S, Hooton TM, Stamm WE. Chromosomal
985 restriction fragment length polymorphism analysis of *Escherichia coli* strains causing

986 recurrent urinary tract infections in young women. J Infect Dis. 1995;172(2):440-5. Epub
987 1995/08/01. doi: 10.1093/infdis/172.2.440. PubMed PMID: 7622887.
988 55. Russell CW, Fleming BA, Jost CA, Tran A, Stenquist AT, Wambaugh MA, et al.
989 Context-Dependent Requirements for FimH and Other Canonical Virulence Factors in
990 Gut Colonization by Extraintestinal Pathogenic *Escherichia coli*. Infection and Immunity.
991 2018;86(3). Epub 2018/01/10. doi: 10.1128/IAI.00746-17. PubMed PMID: 29311232;
992 PubMed Central PMCID: PMCPMC5820936.
993 56. Russell CW, Mulvey MA. The Extraintestinal Pathogenic *Escherichia coli* Factor
994 RqlI Constrains the Genotoxic Effects of the RecQ-Like Helicase RqlH. PLoS Pathog.
995 2015;11(12):e1005317. doi: 10.1371/journal.ppat.1005317. PubMed PMID: 26636713;
996 PubMed Central PMCID: PMCPMC4670107.
997 57. Russell CW, Richards AC, Chang AS, Mulvey MA. The Rhomboid Protease
998 GlpG Promotes the Persistence of Extraintestinal Pathogenic *Escherichia coli* within the
999 Gut. Infection and Immunity. 2017;85(6). Epub 2017/04/05. doi: 10.1128/IAI.00866-16.
1000 PubMed PMID: 28373355; PubMed Central PMCID: PMCPMC5442614.
1001 58. Lewis AJ, Richards AC, Mulvey MA. Invasion of Host Cells and Tissues by
1002 Uropathogenic Bacteria. Microbiol Spectr. 2016;4(6). Epub 2017/01/15. doi:
1003 10.1128/microbiolspec.UTI-0026-2016. PubMed PMID: 28087946; PubMed Central
1004 PMCID: PMCPMC5244466.
1005 59. Hagberg L, Hull R, Hull S, McGhee JR, Michalek SM, Svanborg Eden C.
1006 Difference in susceptibility to gram-negative urinary tract infection between C3H/HeJ
1007 and C3H/HeN mice. Infection and Immunity. 1984;46(3):839-44.
1008 60. Suhs KA, Marthaler BR, Welch RA, Hopkins WJ. Lack of association between
1009 the Tlr4 (Lpsd/Lpsd) genotype and increased susceptibility to *Escherichia coli* bladder
1010 infections in female C3H/HeJ mice. MBio. 2011;2(3):e00094-11. Epub 2011/06/02. doi:
1011 10.1128/mBio.00094-11 e00094-11 [pii] mBio.00094-11 [pii]. PubMed PMID: 21628500;
1012 PubMed Central PMCID: PMC3104495.
1013 61. Hopkins WJ, Elkahwaji J, Kendziorski C, Moser AR, Briggs PM, Suhs KA.
1014 Quantitative trait loci associated with susceptibility to bladder and kidney infections
1015 induced by *Escherichia coli* in female C3H/HeJ mice. J Infect Dis. 2009;199(3):355-61.

Epub 2008/12/09. doi: 10.1086/595987. PubMed PMID: 19061424; PubMed Central PMCID: PMC2683358.

62. Donovan GT, Norton JP, Bower JM, Mulvey MA. Adenylate cyclase and the cyclic AMP receptor protein modulate stress resistance and virulence capacity of uropathogenic *Escherichia coli*. Infection and Immunity. 2013;81(1):249-58. Epub 2012/11/02. doi: 10.1128/iai.00796-12. PubMed PMID: 23115037; PubMed Central PMCID: PMCPMC3536135.

63. van der Mee-Marquet NL, Blanc DS, Gbaguidi-Haore H, Dos Santos Borges S, Viboud Q, Bertrand X, et al. Marked increase in incidence for bloodstream infections due to Escherichia coli, a side effect of previous antibiotic therapy in the elderly. Front Microbiol. 2015;6:646. doi: 10.3389/fmicb.2015.00646. PubMed PMID: 26175721.

64. Picard B, Garcia JS, Gouriou S, Duriez P, Brahimi N, Bingen E, et al. The link between phylogeny and virulence in *Escherichia coli* extraintestinal infection. Infection and immunity. 1999;67(2):546-53. Epub 1999/01/23. doi: 10.1128/IAI.67.2.546-553.1999. PubMed PMID: 9916057; PubMed Central PMCID: PMCPMC96353.

65. Trivedi S, Labuz D, Anderson CP, Araujo CV, Blair A, Middleton EA, et al. Mucosal-associated invariant T (MAIT) cells mediate protective host responses in sepsis. Elife. 2020;9. Epub 2020/11/10. doi: 10.7554/eLife.55615. PubMed PMID: 33164745; PubMed Central PMCID: PMCPMC7679140.

66. Mikkola R, Kurland CG. Evidence for demand-regulation of ribosome accumulation in *E. coli*. Biochimie. 1991;73(12):1551-6. Epub 1991/12/01. PubMed PMID: 1805968.

67. Korshunov S, Imlay JA. Detection and quantification of superoxide formed within the periplasm of *Escherichia coli*. J Bacteriol. 2006;188(17):6326-34. PubMed PMID: 16923900.

68. Bower JM, Mulvey MA. Polyamine-mediated resistance of uropathogenic *Escherichia coli* to nitrosative stress. J Bacteriol. 2006;188(3):928-33. Epub 2006/01/24. doi: 188/3/928 [pii] 10.1128/JB.188.3.928-933.2006. PubMed PMID: 16428396.

69. Woolford G, Casselden RJ, Walters CL. Gaseous products of the interaction of sodium nitrite with procine skeletal muscle. Biochem J. 1972;130(2):82P-3P. Epub

1046 1972/11/01. doi: 10.1042/bj1300082pb. PubMed PMID: 4664608; PubMed Central
1047 PMCID: PMCPMC1174485.
1048 70. Hassan HM, Fridovich I. Superoxide radical and the oxygen enhancement of the
1049 toxicity of paraquat in *Escherichia coli*. J Biol Chem. 1978;253(22):8143-8. Epub
1050 1978/11/25. PubMed PMID: 213429.
1051 71. Withman B, Gunasekera TS, Beesetty P, Agans R, Paliy O. Transcriptional
1052 responses of uropathogenic *Escherichia coli* to increased environmental osmolality
1053 caused by salt or urea. Infection and immunity. 2013;81(1):80-9. Epub 2012/10/24. doi:
1054 10.1128/iai.01049-12. PubMed PMID: 23090957; PubMed Central PMCID:
1055 PMCPMC3536127.
1056 72. Schwan WR. Survival of uropathogenic *Escherichia coli* in the murine urinary
1057 tract is dependent on OmpR. Microbiology. 2009;155(Pt 6):1832-9. Epub 2009/04/23.
1058 doi: mic.0.026187-0 [pii]
1059 10.1099/mic.0.026187-0. PubMed PMID: 19383700.
1060 73. Urbonavicius J, Qian Q, Durand JM, Hagervall TG, Bjork GR. Improvement of
1061 reading frame maintenance is a common function for several tRNA modifications.
1062 EMBO J. 2001;20(17):4863-73. Epub 2001/09/05. doi: 10.1093/emboj/20.17.4863.
1063 PubMed PMID: 11532950; PubMed Central PMCID: PMC125605.
1064 74. Urbonavicius J, Stahl G, Durand JM, Ben Salem SN, Qian Q, Farabaugh PJ, et
1065 al. Transfer RNA modifications that alter +1 frameshifting in general fail to affect -1
1066 frameshifting. RNA (New York, NY). 2003;9(6):760-8. Epub 2003/05/21. PubMed PMID:
1067 12756333; PubMed Central PMCID: PMC1370442.
1068 75. Howard MT, Shirts BH, Zhou J, Carlson CL, Matsufuji S, Gesteland RF, et al.
1069 Cell culture analysis of the regulatory frameshift event required for the expression of
1070 mammalian antizymes. Genes to Cells. 2001;6(11):931-41. Epub 2001/12/26. PubMed
1071 PMID: 11733031.
1072 76. Grentzmann G, Ingram JA, Kelly PJ, Gesteland RF, Atkins JF. A dual-luciferase
1073 reporter system for studying recoding signals. RNA (New York, NY). 1998;4(4):479-86.
1074 Epub 1998/06/18. PubMed PMID: 9630253; PubMed Central PMCID:
1075 PMCPMC1369633.

77. Floyd KA, Moore JL, Eberly AR, Good JA, Shaffer CL, Zaver H, et al. Adhesive fiber stratification in uropathogenic *Escherichia coli* biofilms unveils oxygen-mediated control of type 1 pili. PLoS Pathog. 2015;11(3):e1004697. Epub 2015/03/05. doi: 10.1371/journal.ppat.1004697. PubMed PMID: 25738819; PubMed Central PMCID: PMCPMC4349694.

78. Beebout CJ, Eberly AR, Werby SH, Reasoner SA, Brannon JR, De S, et al. Respiratory Heterogeneity Shapes Biofilm Formation and Host Colonization in Uropathogenic *Escherichia coli*. MBio. 2019;10(2). Epub 2019/04/04. doi: 10.1128/mBio.02400-18. PubMed PMID: 30940709; PubMed Central PMCID: PMCPMC6445943.

79. Wolf J, Gerber AP, Keller W. tadA, an essential tRNA-specific adenosine deaminase from *Escherichia coli*. EMBO J. 2002;21(14):3841-51. Epub 2002/07/12. doi: 10.1093/emboj/cdf362. PubMed PMID: 12110595; PubMed Central PMCID: PMCPMC126108.

80. Bar-Yaacov D, Mordret E, Towers R, Biniashvili T, Soyris C, Schwartz S, et al. RNA editing in bacteria recodes multiple proteins and regulates an evolutionarily conserved toxin-antitoxin system. Genome Res. 2017;27(10):1696-703. Epub 2017/09/03. doi: 10.1101/gr.222760.117. PubMed PMID: 28864459; PubMed Central PMCID: PMCPMC5630033.

81. Kulesus RR, Diaz-Perez K, Slechta ES, Eto DS, Mulvey MA. Impact of the RNA chaperone Hfq on the fitness and virulence potential of uropathogenic *Escherichia coli*. Infection and Immunity. 2008;76(7):3019-26. Epub 2008/05/07. doi: IAI.00022-08 [pii] 10.1128/IAI.00022-08. PubMed PMID: 18458066.

82. Endres L, Dedon PC, Begley TJ. Codon-biased translation can be regulated by wobble-base tRNA modification systems during cellular stress responses. RNA biology. 2015;12(6):603-14. Epub 2015/04/22. doi: 10.1080/15476286.2015.1031947. PubMed PMID: 25892531; PubMed Central PMCID: PMCPMC4615639.

83. Koh CS, Sarin LP. Transfer RNA modification and infection - Implications for pathogenicity and host responses. Biochim Biophys Acta Gene Regul Mech. 2018;1861(4):419-32. Epub 2018/01/30. doi: 10.1016/j.bbagrm.2018.01.015. PubMed PMID: 29378328.

84. Durand JM, Bjork GR, Kuwae A, Yoshikawa M, Sasakawa C. The modified nucleoside 2-methylthio-N6-isopentenyladenosine in tRNA of *Shigella flexneri* is required for expression of virulence genes. J Bacteriol. 1997;179(18):5777-82. Epub 1997/09/19. doi: 10.1128/jb.179.18.5777-5782.1997. PubMed PMID: 9294434; PubMed Central PMCID: PMCPMC179466.

85. Tsui HC, Winkler ME. Transcriptional patterns of the mutL-miaA superoperon of *Escherichia coli* K-12 suggest a model for posttranscriptional regulation. Biochimie. 1994;76(12):1168-77. Epub 1994/01/01. doi: 10.1016/0300-9084(94)90046-9. PubMed PMID: 7748952.

86. Connolly DM, Winkler ME. Structure of *Escherichia coli* K-12 miaA and characterization of the mutator phenotype caused by *miaA* insertion mutations. J Bacteriol. 1991;173(5):1711-21. Epub 1991/03/01. doi: 10.1128/jb.173.5.1711-1721.1991. PubMed PMID: 1999389; PubMed Central PMCID: PMCPMC207322.

87. Dedon PC, Begley TJ. A system of RNA modifications and biased codon use controls cellular stress response at the level of translation. Chemical Research in Toxicology. 2014;27(3):330-7. Epub 2014/01/16. doi: 10.1021/tx400438d. PubMed PMID: 24422464; PubMed Central PMCID: PMCPMC3997223.

88. Chan CT, Pang YL, Deng W, Babu IR, Dyavaiah M, Begley TJ, et al. Reprogramming of tRNA modifications controls the oxidative stress response by codon-biased translation of proteins. Nature Comm. 2012;3:937. Epub 2012/07/05. doi: 10.1038/ncomms1938. PubMed PMID: 22760636; PubMed Central PMCID: PMCPMC3535174.

89. Rehl JM, Shippy DC, Eakley NM, Brevik MD, Sand JM, Cook ME, et al. GidA expression in *Salmonella* is modulated under certain environmental conditions. Curr Microbiol. 2013;67(3):279-85. Epub 2013/04/13. doi: 10.1007/s00284-013-0361-2. PubMed PMID: 23579313.

90. Pollo-Oliveira L, de Crecy-Lagard V. Can Protein Expression Be Regulated by Modulation of tRNA Modification Profiles? Biochemistry. 2019;58(5):355-62. Epub 2018/12/05. doi: 10.1021/acs.biochem.8b01035. PubMed PMID: 30511849; PubMed Central PMCID: PMCPMC6363828.

1137 91. Wong GT, Bonocora RP, Schep AN, Beeler SM, Lee Fong AJ, Shull LM, et al.
1138 Genome-Wide Transcriptional Response to Varying RpoS Levels in *Escherichia coli* K-
1139 12. J Bacteriol. 2017;199(7). Epub 2017/01/25. doi: 10.1128/JB.00755-16. PubMed
1140 PMID: 28115545; PubMed Central PMCID: PMCPMC5350281.
1141 92. Battesti A, Majdalani N, Gottesman S. The RpoS-mediated general stress
1142 response in *Escherichia coli*. Annu Rev Microbiol. 2011;65:189-213. Epub 2011/06/07.
1143 doi: 10.1146/annurev-micro-090110-102946. PubMed PMID: 21639793.
1144 93. Chao Y, Papenfort K, Reinhardt R, Sharma CM, Vogel J. An atlas of Hfq-bound
1145 transcripts reveals 3' UTRs as a genomic reservoir of regulatory small RNAs. EMBO J.
1146 2012;31(20):4005-19. Epub 2012/08/28. doi: 10.1038/emboj.2012.229. PubMed PMID:
1147 22922465; PubMed Central PMCID: PMCPMC3474919.
1148 94. Pan T. Adaptive translation as a mechanism of stress response and adaptation.
1149 Annual Review of Genetics. 2013;47:121-37. Epub 2013/08/31. doi: 10.1146/annurev-
1150 genet-111212-133522. PubMed PMID: 23988117; PubMed Central PMCID:
1151 PMCPMC4109725.
1152 95. Drummond DA, Wilke CO. The evolutionary consequences of erroneous protein
1153 synthesis. Nat Rev Genet. 2009;10(10):715-24. doi: 10.1038/nrg2662. PubMed PMID:
1154 19763154; PubMed Central PMCID: PMCPMC2764353.
1155 96. Moura GR, Carreto LC, Santos MA. Genetic code ambiguity: an unexpected
1156 source of proteome innovation and phenotypic diversity. Curr Opin Microbiol.
1157 2009;12(6):631-7. doi: 10.1016/j.mib.2009.09.004. PubMed PMID: 19853500.
1158 97. Mohler K, Ibba M. Translational fidelity and mistranslation in the cellular response
1159 to stress. Nature Microbiology. 2017;2:17117. Epub 2017/08/25. doi:
1160 10.1038/nmicrobiol.2017.117. PubMed PMID: 28836574; PubMed Central PMCID:
1161 PMCPMC5697424.
1162 98. Blango MG, Mulvey MA. Persistence of uropathogenic *Escherichia coli* in the
1163 face of multiple antibiotics. Antimicrob Agents Chemother. 2010;54(5):1855-63. Epub
1164 2010/03/17. doi: AAC.00014-10 [pii] 10.1128/AAC.00014-10. PubMed PMID: 20231390;
1165 PubMed Central PMCID: PMC2863638.
1166 99. Mulvey MA, Lopez-Boado YS, Wilson CL, Roth R, Parks WC, Heuser J, et al.
1167 Induction and evasion of host defenses by type 1-piliated uropathogenic *Escherichia*

coli. Science (New York, NY). 1998;282(5393):1494-7. Epub 1998/11/20. PubMed PMID: 9822381.

100. Blango MG, Ott EM, Erman A, Veranic P, Mulvey MA. Forced resurgence and targeting of intracellular uropathogenic *Escherichia coli* reservoirs. PloS One. 2014;9(3):e93327. Epub 2014/03/29. doi: 10.1371/journal.pone.0093327. PubMed PMID: 24667805; PubMed Central PMCID: PMCPMC3965547.

101. Parkinson JS. cheA, cheB, and cheC genes of *Escherichia coli* and their role in chemotaxis. J Bacteriol. 1976;126(2):758-70. Epub 1976/05/01. doi: 10.1128/JB.126.2.758-770.1976. PubMed PMID: 770453; PubMed Central PMCID: PMCPMC233211.

102. Eto DS, Gordon HB, Dhakal BK, Jones TA, Mulvey MA. Clathrin, AP-2, and the NPXY-binding subset of alternate endocytic adaptors facilitate FimH-mediated bacterial invasion of host cells. Cellular Microbiology. 2008;10(12):2553-67. Epub 2008/08/30. doi: 10.1111/j.1462-5822.2008.01229.x. PubMed PMID: 18754852.

103. Miles ZD, Myers WK, Kincannon WM, Britt RD, Bandarian V. Biochemical and Spectroscopic Studies of Epoxyqueuosine Reductase: A Novel Iron-Sulfur Cluster- and Cobalamin-Containing Protein Involved in the Biosynthesis of Queuosine. Biochemistry. 2015;54(31):4927-35. Epub 2015/08/01. doi: 10.1021/acs.biochem.5b00335. PubMed PMID: 26230193; PubMed Central PMCID: PMCPMC4753064.

104. Miles ZD, McCarty RM, Molnar G, Bandarian V. Discovery of epoxyqueuosine (oQ) reductase reveals parallels between halorespiration and tRNA modification. Proc Natl Acad Sci U S A. 2011;108(18):7368-72. Epub 2011/04/20. doi: 10.1073/pnas.1018636108. PubMed PMID: 21502530; PubMed Central PMCID: PMCPMC3088584.

105. Keseler IM, Mackie A, Santos-Zavaleta A, Billington R, Bonavides-Martinez C, Caspi R, et al. The EcoCyc database: reflecting new knowledge about *Escherichia coli* K-12. Nucleic acids research. 2017;45(D1):D543-D50. Epub 2016/12/03. doi: 10.1093/nar/gkw1003. PubMed PMID: 27899573; PubMed Central PMCID: PMCPMC5210515.

106. Szklarczyk D, Gable AL, Lyon D, Junge A, Wyder S, Huerta-Cepas J, et al. STRING v11: protein-protein association networks with increased coverage, supporting

1199 functional discovery in genome-wide experimental datasets. Nucleic Acids Research.
1200 2019;47(D1):D607-D13. Epub 2018/11/27. doi: 10.1093/nar/gky1131. PubMed PMID:
1201 30476243; PubMed Central PMCID: PMCPMC6323986.
1202 107. Kelley LA, Mezulis S, Yates CM, Wass MN, Sternberg MJ. The Phyre2 web
1203 portal for protein modeling, prediction and analysis. Nat Protoc. 2015;10(6):845-58.
1204 Epub 2015/05/08. doi: 10.1038/nprot.2015.053. PubMed PMID: 25950237; PubMed
1205 Central PMCID: PMCPMC5298202.
1206 108. Mulvey MA, Schilling JD, Hultgren SJ. Establishment of a persistent *Escherichia*
1207 *coli* reservoir during the acute phase of a bladder infection. Infection and Immunity.
1208 2001;69(7):4572-9. PubMed PMID: 11402001.
1209 109. Guzman LM, Belin D, Carson MJ, Beckwith J. Tight regulation, modulation, and
1210 high-level expression by vectors containing the arabinose PBAD promoter. J Bacteriol.
1211 1995;177(14):4121-30. Epub 1995/07/01. doi: 10.1128/jb.177.14.4121-4130.1995.
1212 PubMed PMID: 7608087; PubMed Central PMCID: PMCPMC177145.
1213 110. Zhou Q, Ames P, Parkinson JS. Mutational analyses of HAMP helices suggest a
1214 dynamic bundle model of input-output signalling in chemoreceptors. Mol Microbiol.
1215 2009;73(5):801-14. Epub 2009/08/07. doi: 10.1111/j.1365-2958.2009.06819.x. PubMed
1216 PMID: 19656294; PubMed Central PMCID: PMCPMC2749569.
1217

FIGURE LEGENDS

Figure 1. MiaA promotes ExPEC fitness and virulence within diverse host niches.

(**A**) MiaA and MiaB act sequentially to modify tRNA molecules that recognize UNN codons; modified from [37]. DMAPP, dimethylallyl diphosphate; SAM, S-adenosylmethionine; SAH, S-adenosylhomocysteine; Cys, cysteine.

(**B** and **C**) To assess gut colonization, adult BALB/c mice were inoculated via oral gavage with ~10^9 CFU of a 1:1 mixture of (**B**) UTI89 and UTI89Δ*miaA* or (**C**) UTI89 and UTI89Δ*miaB.* Fecal titers were determined at the indicated time points and used to calculate competitive indices (CI). ***, $P < 0.001$; ****, $P < 0.0001$ by one sample *t*-tests. n = 7-8 mice from two independent experiments.

(**D**) The bladders of adult female CBA/J mice were inoculated via transurethral catheterization with ~10^7 CFU of UTI89, UTI89Δ*miaA*, or UTI89Δ*miaB*. Mice were sacrificed 3 days later and bacterial titers within the bladders were determined by plating tissue homogenates. **, $P < 0.01$ by Mann Whitney U tests; $n \geq 19$ mice per group from at least three independent experiments. In B, C, and D, bars indicate median values; dots represent individual mice.

(**E**) Kaplan Meier survival curves of C57Bl/6 mice inoculated via i.p. injections with ~10^7 CFU of UTI89 (black line), UTI89Δ*miaA* (blue), or UTI89Δ*miaB* (orange). ****, $P < 0.0001$ by Log-rank Mantel Cox test for UTI89 versus UTI89Δ*miaA*; n = 13 mice per group from two independent experiments.

Figure 1

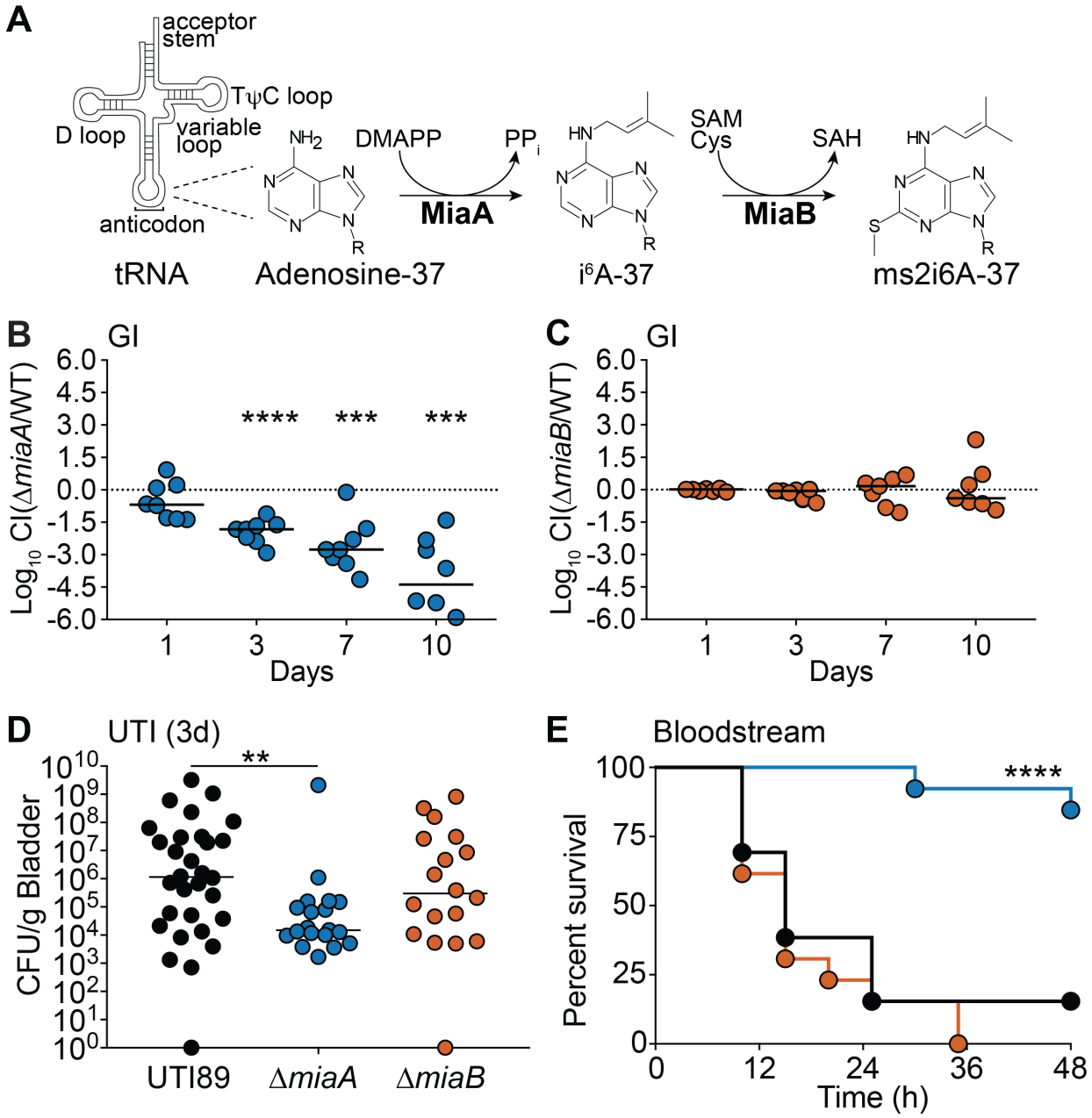

Figure 2. Deletion of *miaA* limits growth of UTI89 in rich medium and lowers resistance to oxidative and nitrosative stress.

(**A-F**) Graphs indicate mean growth of UTI89, UTI89Δ*miaA*, and UTI89Δ*miaB* in shaking cultures with modified M9 media, LB, MES-LB, MES-LB with 1 or 2 mM ASN, or LB with 1 mM MV.

(**G** and **H**) Curves show mean growth of UTI89 and UTI89Δ*miaA* carrying pMiaA$_{nat}$ (with *miaA* expressed from its native promoter) or the empty vector control pACYC184 in LB containing (G) 2 mM ASN or (H) 1 mM MV.

Each curve shows the means of results from four replicates, and are representative of three independent experiments.

Figure 2

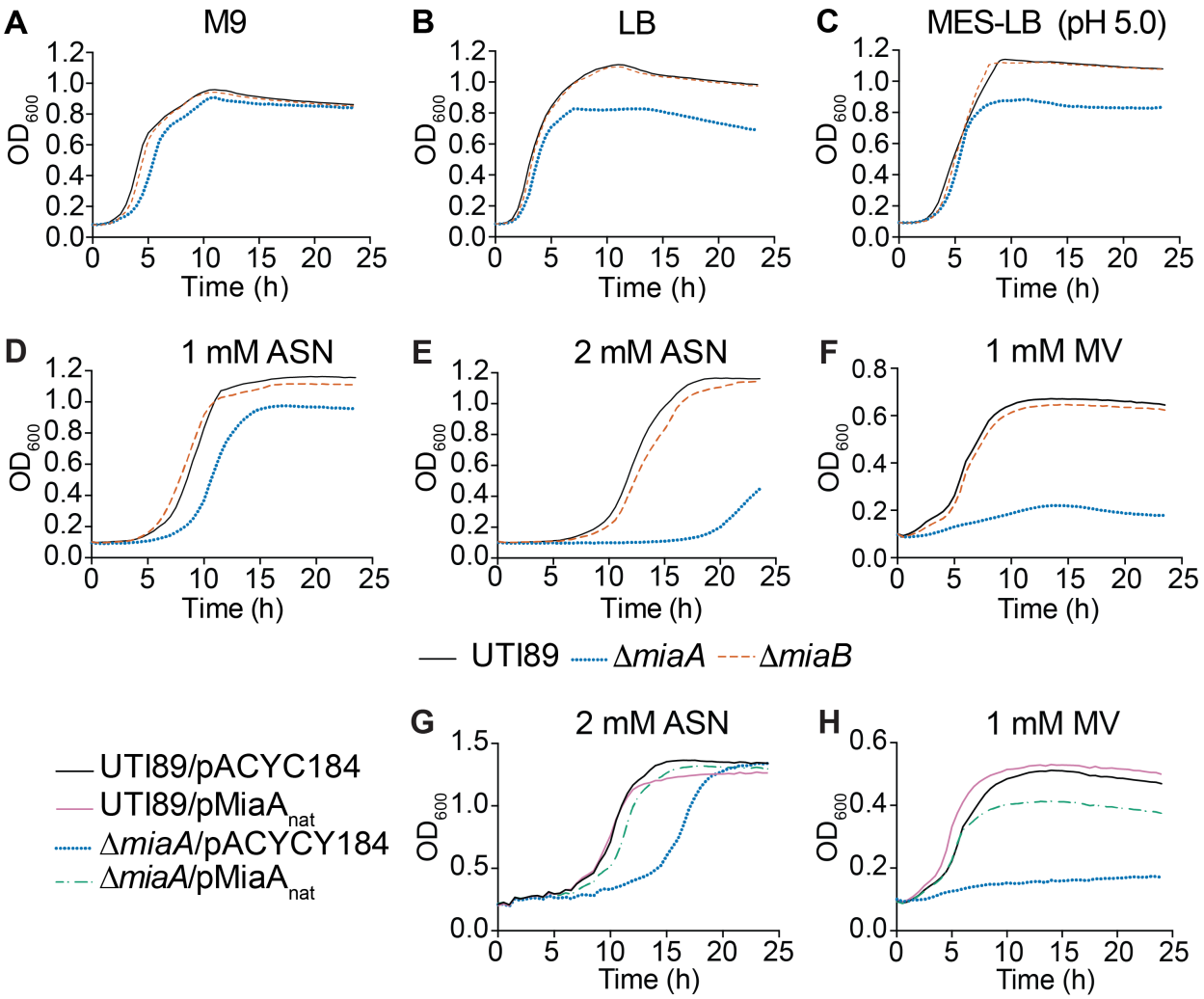

Figure 3. MiaA enhances the resistance of UTI89 to osmotic stress.

(**A**) Bacteria were grown to stationary phase in LB, pelleted, and resuspended in ddH_2O. The mean numbers (±SEM) of surviving bacteria recovered at the indicated time points are graphed as the percentage of the bacteria present immediately after resuspension in ddH_2O (time 0). *P*-values were determined by two-way ANOVA with the Geisser-Greenhouse correction; n = 3 independent assays each done in triplicate.

(**B**) Bars indicate mean numbers of bacteria (±SD) that survived 2 hours in ddH_2O with 0.1% glucose, calculated as a percent of the inoculum. *P* values were determined, relative to the control strain UTI89/pMiaA$_{nat}$, by unpaired *t*-tests with Welch's correction; n = 3 independent assays.

(**C** and **D**) Curves show growth of the indicated strains in LB plus 5% NaCl, as measured by OD_{600}. Data are representative of at least three independent experiments performed in quadruplicate.

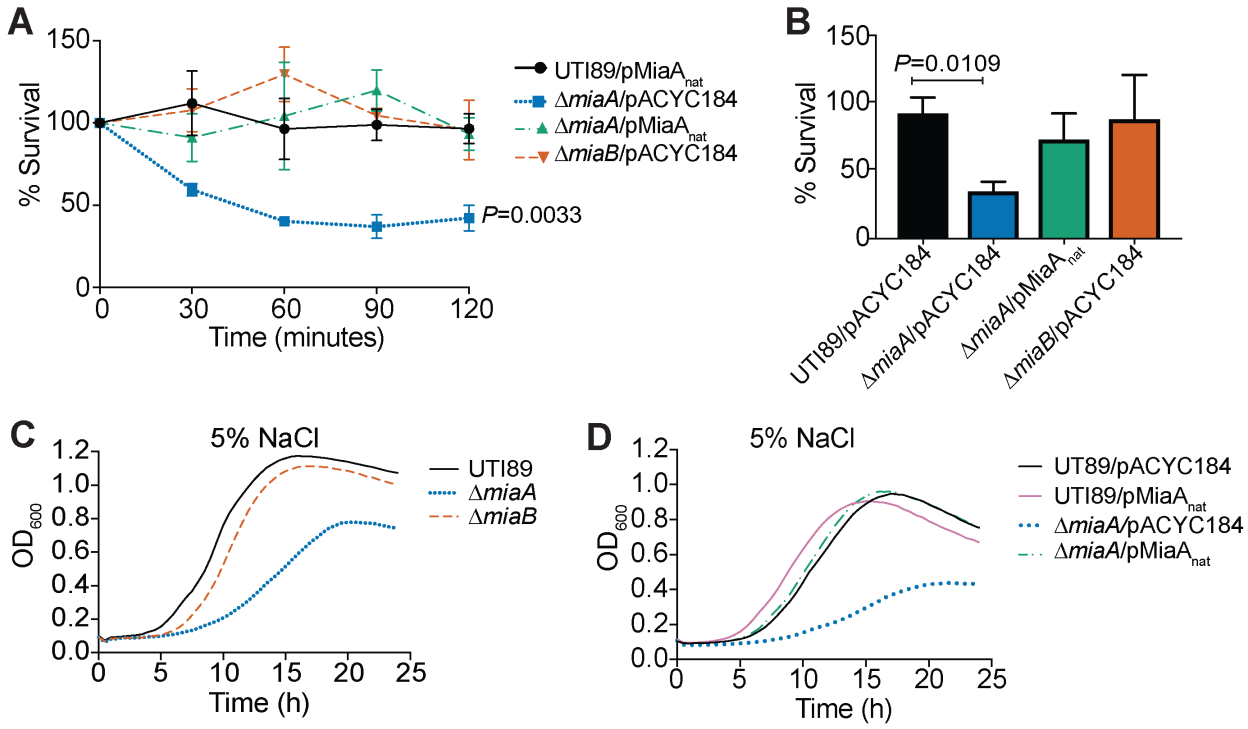

Figure 4. High salt stress downregulates MiaA translation and reduces ms^2i^6A levels.

(**A**) Top panel shows schematic of the experimental setup. UTI89/pMiaA-$Flag_{nat}$ was diluted from overnight cultures into fresh LB and grown shaking for 2.5 hours at 37˚C prior to resuspension in LB or LB + 5% NaCl. Incubations were continued for the indicated times before samples were collected and analyzed by western blots using anti-Flag and anti-*E. coli* (loading control) antibodies (bottom panel).

(**B**) Top panel summarizes the experimental setup. Overnight cultures of UTI89/pMiaA-$Flag_{nat}$ were diluted directly into fresh LB or LB + 5% NaCl and grown shaking to OD_{600} of 0.5 prior to processing for western blot analysis (bottom panel).

(**C and D**) UTI89 from mid-logarithmic cultures in LB was resuspended in LB or LB + 5% NaCl and one hour later the evels of *miaA* and *miaB* transcripts were determined by RT-qPCR. Bars indicate mean values from 9 independent replicates, each with two technical replicates. *, $P < 0.05$; ***, $P < 0.001$ by Mann-Whitney U tests.

(**E and F**) Graphs show relative levels of i^6A and ms^2i^6A recovered from UTI89 and UTI89Δ*miaA* following growth to OD_{600} of 0.5 in LB or LB + 5% NaCl, as determined by LC-MS. **, $P < 0.01$; ***, $P < 0.001$; ****, $P < 0.0001$ by unpaired *t* tests. Bars indicate median values from 4 to 6 independent replicates.

Figure 4

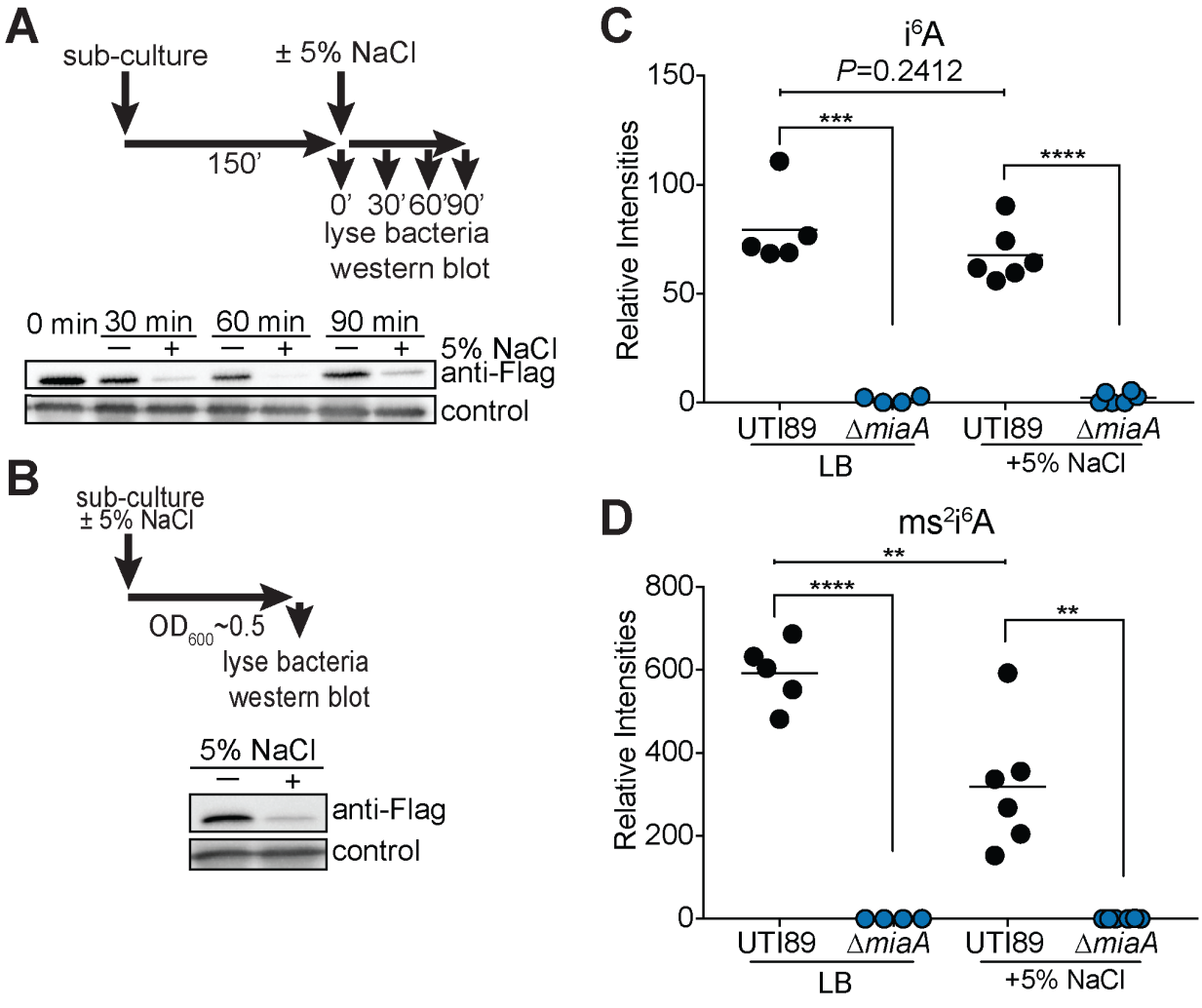

Figure 5. Overexpression of MiaA reduces ExPEC stress resistance.

(**A**) Relative levels of i^6A and ms^2i^6A in UTI89 carrying either pMiaA$_{Ptac}$ or the empty vector control pRR48 following growth to OD_{600} of 0.5 in LB with 1 mM IPTG, as quantified by LC-MS. ****, $P < 0.0001$ by unpaired *t* test; n = 5 to 6 independent replicates per group. (**B-F**) Curves depict growth of UTI89 carrying pMiaA$_{Ptac}$ or the empty vector control pRR48 in LB, LB + 5% NaCl, LB + 1mM MV, MES-LB, or MES-LB + 1 mM ASN. Cultures were grown shaking at 37°C with IPTG added in ten-fold increments from 0 to 1000 μM, as indicated. Each curve depicts the means of results from a single experiment and is representative of at least three independent experiments carried out in quadruplicate.

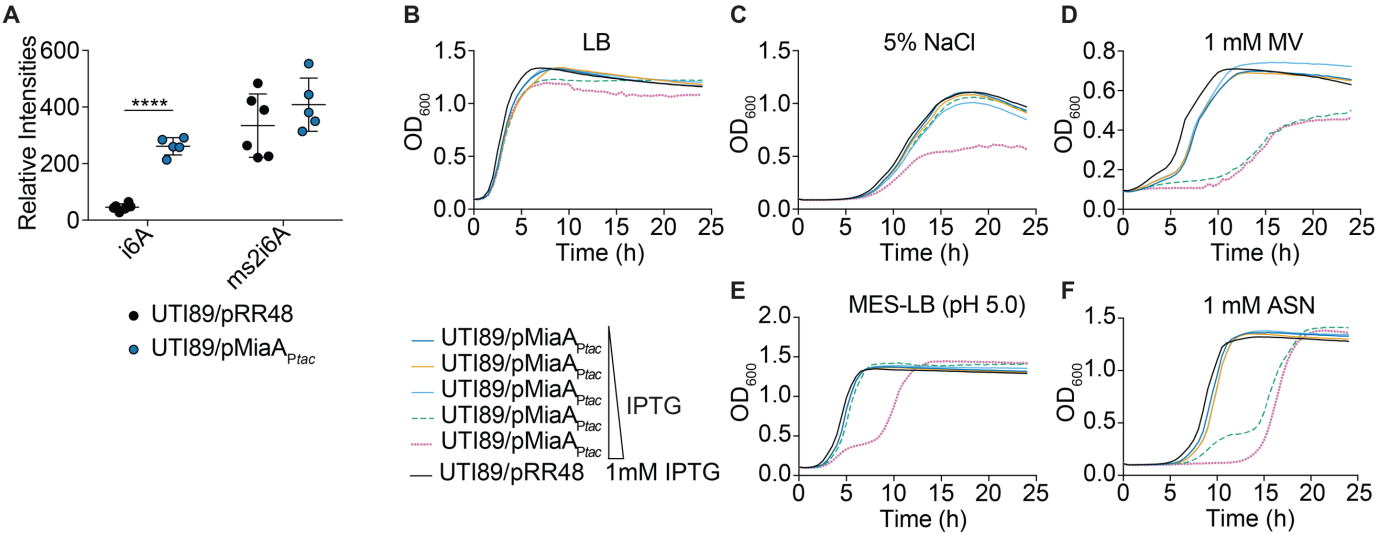

Figure 6. Changing levels of MiaA increase frameshifting.

(**A**) Diagram depicts the structures of the dual luciferase reporters, with specific intergenic linker sequences and premature stop codons (underlined red) indicated below. Each linker contains MiaA-sensitive UNN codons.

(**B and C**) Graphs show results from +1 and -1 frameshifting assays with UTI89, UTI89Δ*miaA*, UTI89/pRR48, or UTI89/pMiaA$_{P\mathit{tac}}$ carrying one of the dual luciferase reporter constructs. Bacteria were grown shaking at 37°C in LB, with 1 mM IPTG included for UTI89/pRR48 and UTI89/pMiaA$_{P\mathit{tac}}$. After reaching an OD_{600} of ~0.2, 0.2% arabinose was added to induce expression of the luciferases. At an OD_{600} of 0.5, translational error rates were quantified by determining the ratio of firefly to renilla luciferase activities in bacteria carrying the +1 (Az1) and -1 (HIV) reporter constructs. Results were normalized using the ratio of firefly to renilla luciferase activity in bacteria carrying control plasmids in which the luciferases are in-frame. **, $P < 0.01$; ****, $P < 0.0001$ by two-tailed unpaired *t* tests; $n = 10$-14 independent replicates.

Figure 6

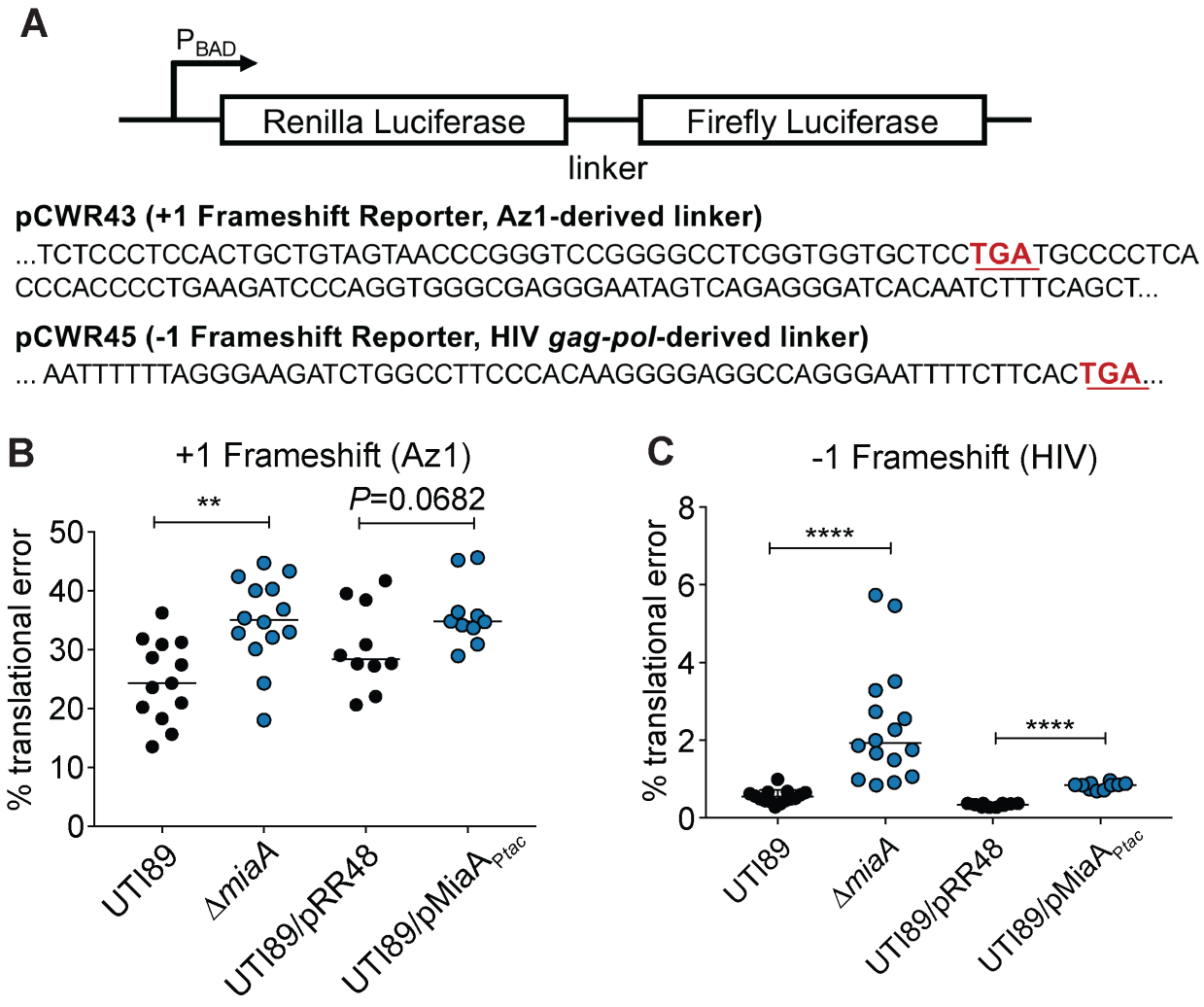

Figure 7. Altering MiaA levels changes the spectrum of expressed proteins.

(**A and B**) Venn diagrams indicate numbers of unique and shared proteins detected in wild-type UTI89 versus UTI89Δ*miaA*, or in UTI89/pRR48 versus UTI89/pMiaA$_{Ptac}$, following growth to OD_{600} of 0.5 in LB. IPTG (1 mM) was included in the UTI89/pRR48 and UTI89/pMiaA$_{Ptac}$ cultures. Relative protein levels were determined by MudPIT.

(**C and D**) Volcano plots show relative protein levels (Log2-fold change) versus P-values (-Log10). Proteins from UTI89Δ*miaA* were quantified relative to the wild-type strain, while proteins levels from UTI89/pMiaA$_{Ptac}$ were assessed relative to UTI89/pRR48. The vertical dotted lines denote a 2-fold change, while the horizontal dotted lines indicate a *P*-value of 0.05. Blue dots indicate proteins that were significantly changed ($P<0.05$) by at least 2-fold. *P* values were determined by Student's *t* tests; $n = 4$ independent replicates for each group.

Figure 7

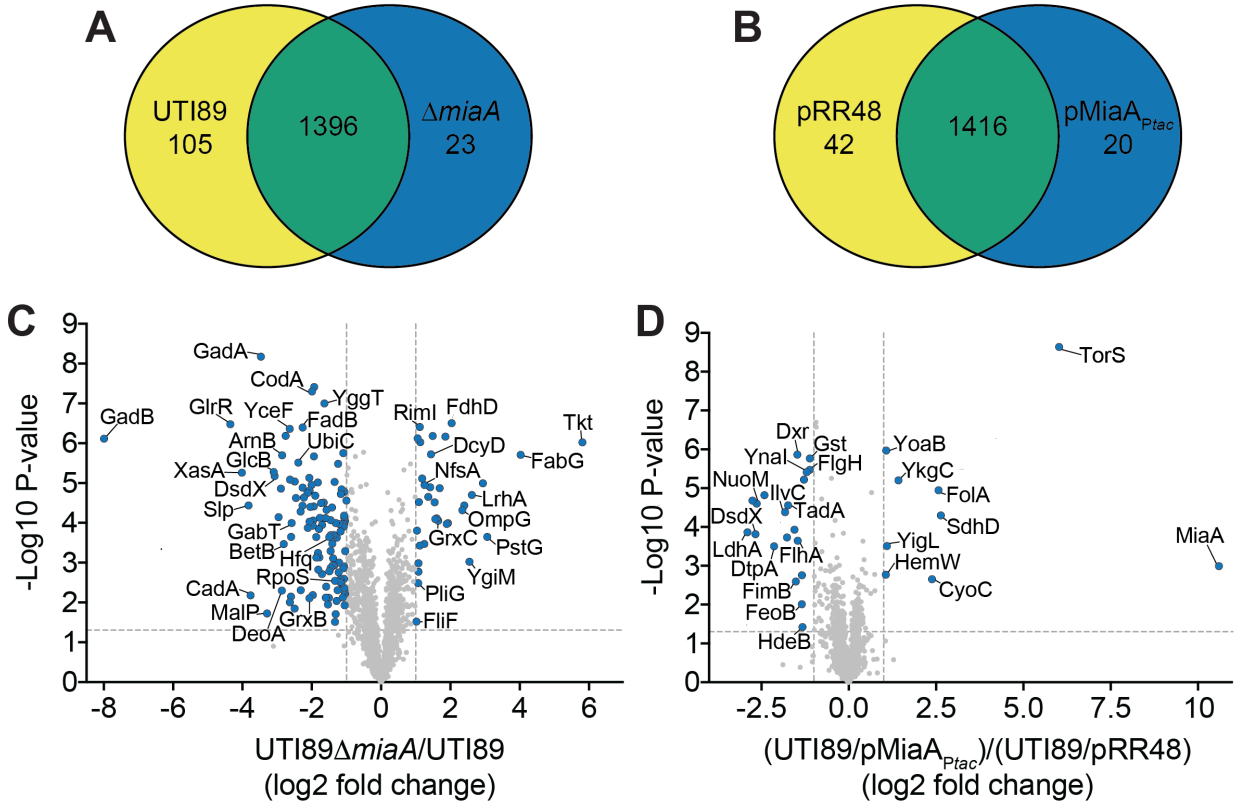

1316 **Figure 8. MiaA regulates ExPEC biofilm development.**

1317 Images show biofilms formed by wild-type UTI89 and its derivatives after 14 days of

1318 growth at room temperature on YESCA plates. Photos are representative of at least three

1319 independent replicates. Scale bar, 1 cm.

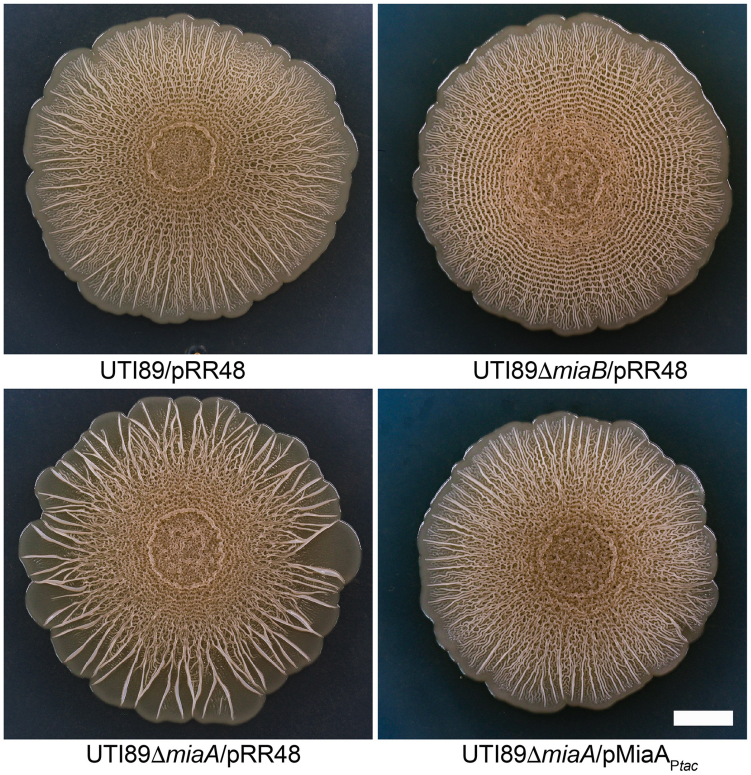

Figure 9. UNN-Leu codon usage ratios vary among MiaA-sensitive transcripts. (**A and B**) Plots show relative protein levels (Log2-fold change) versus UNN-Leu codon usage ratios (UNN Leu/total Leu codons per open reading frame). Proteins in (A) UTI89Δ*miaA* were quantified by MudPIT relative to wild-type UTI89, while proteins levels in (B) UTI89/pMiaA$_{Ptac}$ were calculated relative to UTI89/pRR48, as in Fig. 7. Purple dots denote proteins that were significantly changed (P<0.05, by Student's t tests) by at least 2-fold in UTI89Δ*miaA* or UTI89/pMiaA$_{Ptac}$ relative to their controls. The vertical dotted lines are placed at the 2-fold change cutoffs. The green and black horizontal dashed lines indicate the average ratios of UNN-Leu codons relative to total Leu codons for all open reading frames encoded by the K-12 strain MG1655 and UTI89, respectively.

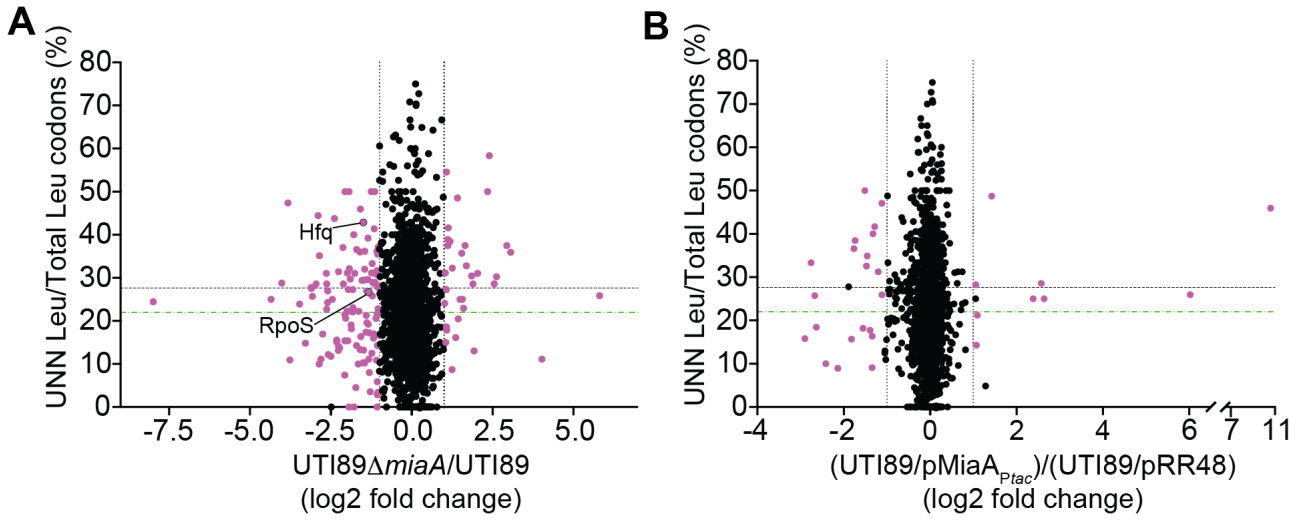

SUPPLEMENTAL INFORMATION

Supplemental Figure S1: MiaA and MiaB do not affect the ability of ExPEC to bind, invade, or persist intracellularly within bladder epithelial cells.

Human bladder epithelial cells (5637 cells) were infected with UTI89, UTI89Δ*miaA*, or UTI89Δ*miaB* for 2 h, followed by a second 2-h incubation in the presence of the bactericidal, host cell-impermeable antibiotic gentamicin (100 μg/ml). Graphs show (**A**) the levels of host cell-associated bacteria prior to the addition of gentamicin, (**B**) and the relative numbers of intracellular bacteria recovered after the 2-h incubation in media containing gentamicin. (**C**) Longer-term bacterial persistence within the bladder cells was assessed by continued incubation of infected host cells for an additional 12 h with gentamicin. For the longer persistence assays, a submaximal concentration of gentamicin (10 μg/ml) was used to prevent extracellular growth of UPEC while limiting possible leaching of the antibiotic into the host cells. Data are expressed relative to wild-type UTI89, with bars indicating median values from 9 to 18 independent experiments performed in triplicate.

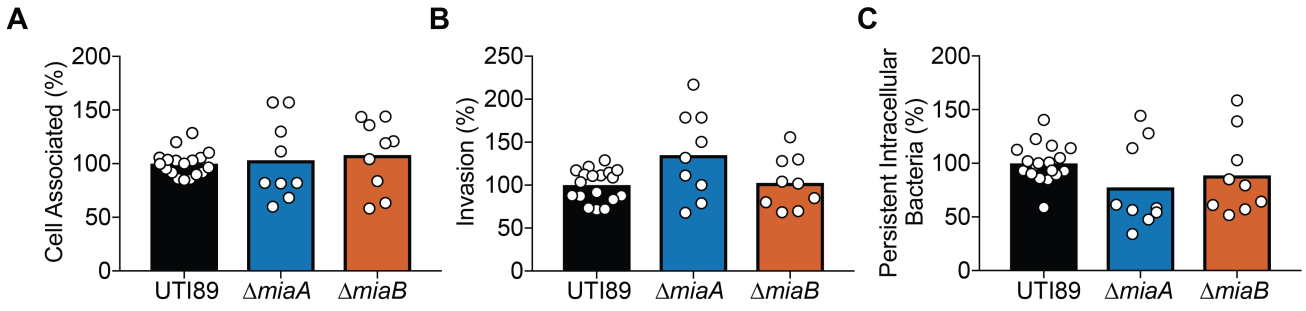

Supplemental Figure S2. MiaA promotes ExPEC colonization and persistence within the murine bladder.

(**A and B**) The bladders of adult female CBA/J mice were inoculated via transurethral injections with ~10^7 CFU of wild-type UTI89 or UTI89Δ*miaA*. Mice were sacrificed (A) 6 hours or (B) 9 days later and bacterial titers within the bladders were determined by plating tissue homogenates.

(**C**) Graph shows bacterial titers recovered from the bladders of adult female C3H/HeJ mice 3 days after inoculation with UTI89 or UTI89Δ*miaA*.

Bars in all graphs denote median values. *, $P < 0.05$ by Mann Whitney U tests; $n \geq 9$ mice per group.

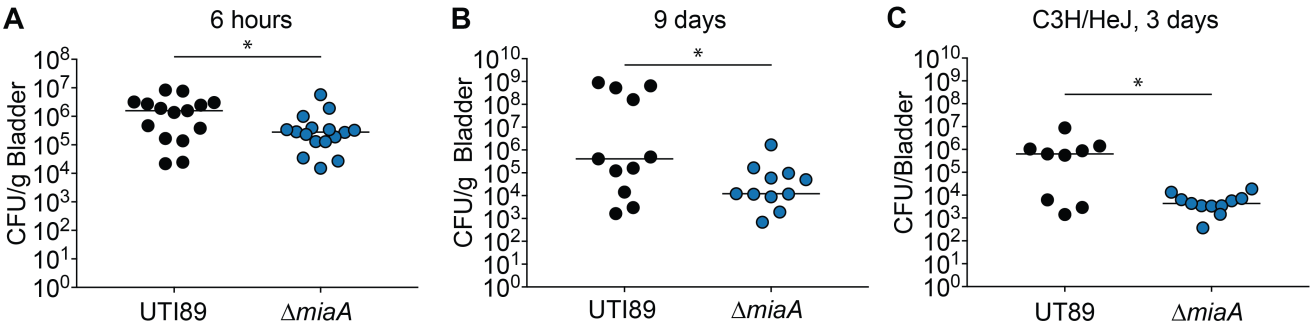

Supplemental Figure S3. MiaA promotes ExPEC fitness in a mouse model of sepsis.

Adult female C57Bl/6 mice were inoculated via i.p. injections with 10^7-10^8 CFU of UTI89, UTI89Δ*miaA*, or UTI89Δ*miaB* and 6 hours later bacterial titers were present in the (**A**) kidneys, (**B**) spleen, and (**C**) liver were determined by plating tissue homogenates. *, $P < 0.05$ and **, $P > 0.01$ by Mann Whitney U tests; $n = 10$ mice per group.

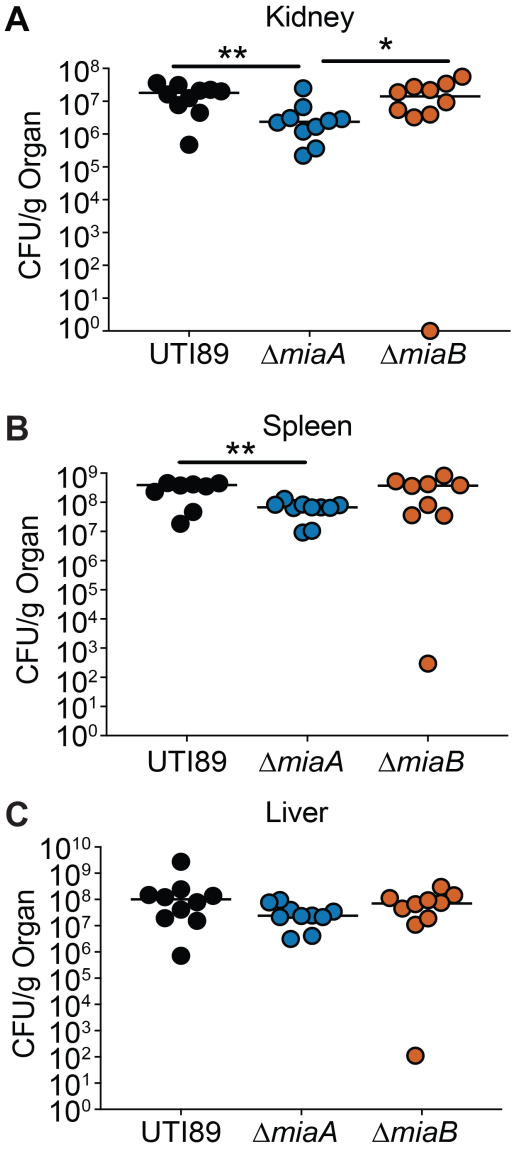

Supplemental Figure S4. The ms^{2}i^{6}A modification is missing in UTI89Δ*miaB*.

RNA was collected from wild-type UTI89 and UTI89Δ*miaB* after reaching an OD_{600} of 0.5 in shaking LB cultures. Relative levels of i^{6}A and ms^{2}i^{6}A were determined by LC-MS. ****, $P < 0.0001$ as determined an unpaired *t* test; n = 5 independent replicates.

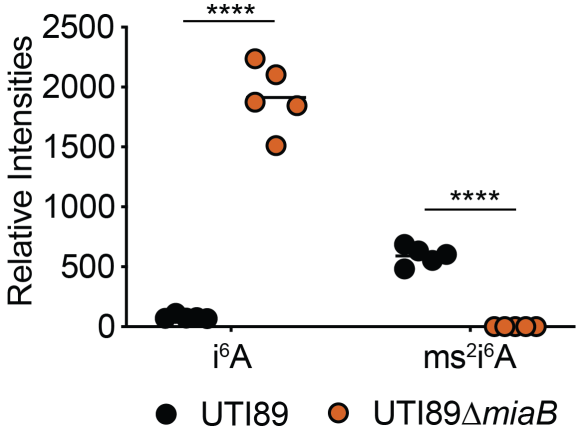

Supplemental Figure S5. Overproduction of MiaB does not affect growth of UTI89 under stressful conditions.

Graphs show growth curves of UTI89 carrying pMiaB$_{Ptac}$ or the control plasmid pRR48 in (**A**) LB, (**B**) 1 mM MV, (**C**) 5% NaCl, (**D**) MES-LB, and (**E**) 1 mM ASN. To overexpress MiaB, 1 mM IPTG was added to UTI89/pMiaB$_{Ptac}$. Data are representative of three or more independent experiments, each done in quadruplicate.

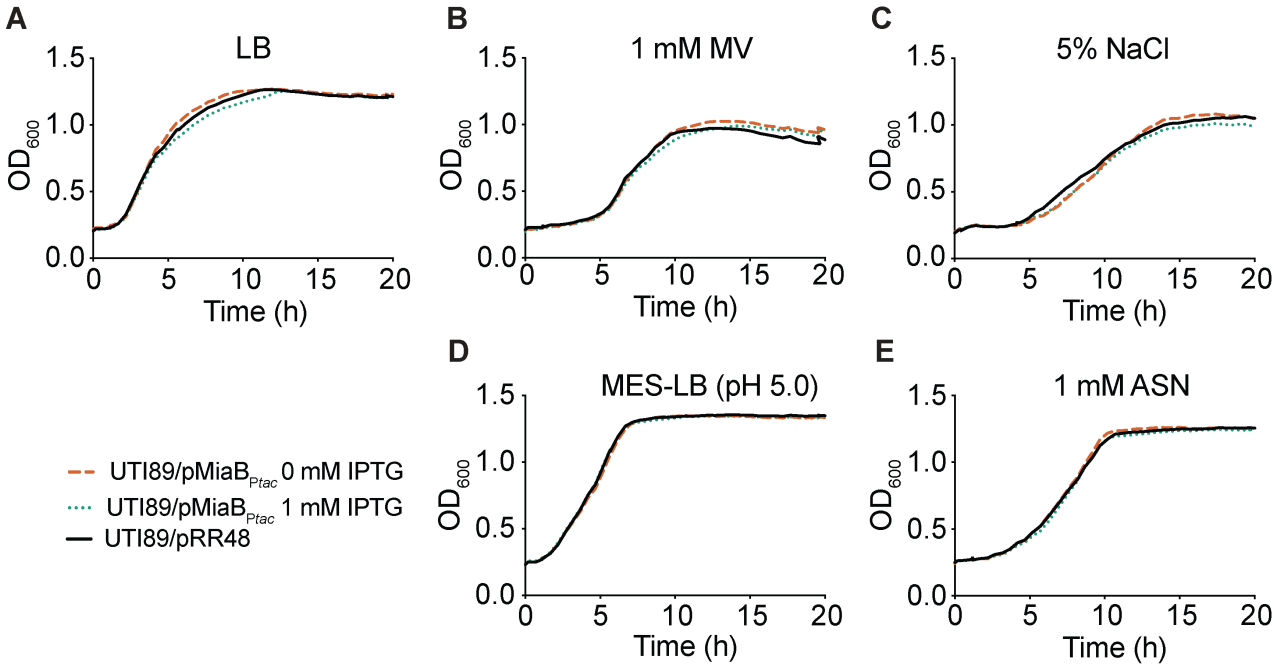

Supplemental Figure S6. MiaA modulates ExPEC motility.

(**A - D**) Graphs indicate the spread of UTI89 (black lines), UTI89Δ*miaA* (dotted blue lines), and UTI89Δ*miaB* (dashed red lines) on (A and C) LB and (B and D) M9 swim motility plates incubated at 37°C. Shown are mean values ± SD from three independent experiments done in triplicate. Swim rates (± SD) for wild-type UTI89 and UTI89Δ*miaA* on LB and M9 swim plates are indicated below the graphs in (A) and (B). *, $P < 0.05$; **; $P < 0.01$; ***, $P < 0.001$; ****, $P < 0.0001$ versus wild-type UTI89, as determined by unpaired *t* tests; n ≥ 4 independent replicates. (**E**) Representative image showing the spread of UTI89/pRR48, UTI89/pMiaB$_{Ptac}$, and UTI89/pMiaA$_{Ptac}$ 6 hours after inoculation onto an LB swim plate containing 1 mM IPTG and ampicillin.

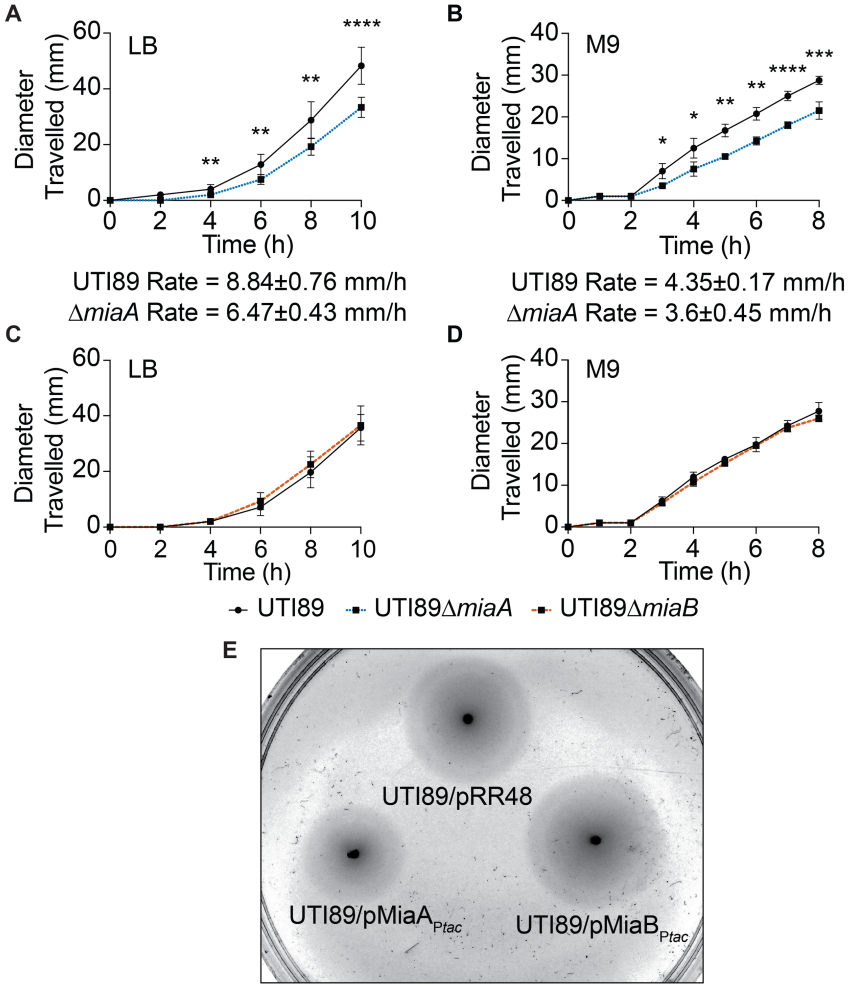

Supplemental Figure S7. UTI89Δ*miaA* is has increased sensitivity to acid stress.

After reaching mid-logarithmic growth phase in LB, wild-type UTI89, UTI89Δ*miaA*, and UTI89Δ*miaB* were exposed to acidic stress (pH 3.0) for 30 min. Following washes in PBS, surviving bacteria were enumerated by dilution plating. Titers are normalized to input. Biological replicates are connected by lines. *, $P < 0.05$ by paired *t* tests.

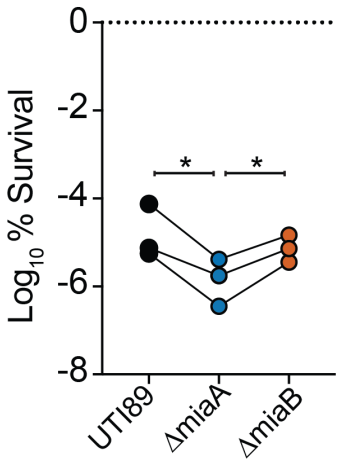

Supplemental Figure S8. Expression of RpoS or Hfq does not rescue growth of UTI89Δ*miaA* in the presence of high salt stress.

(**A - C**) Western blots of RpoS and Flag-tagged Hfq in UTI89 and UTI89Δ*miaA* carrying pRpoS$_{Ptac}$, pHfq$_{Ptac}$, or the empty vector pRR48 following growth to stationary phase in LB or LB with 1 mM IPTG, as indicated. As a loading control, blots were also probed with anti-*E. coli* antibody. A shorter exposure was used for the blot shown in (B), making the RpoS band from UTI89/pRR48 notably lighter than the one shown in (A). Blots are representative of three independent experiments.

(**D and E**) Curves show growth of the UTI89 and UTI89Δ*miaA* with the empty vector pRR48 or plasmids for IPTG-inducible expression of RpoS or Flag-tagged Hfq in LB + 5% NaCl. Cultures were grown shaking at 37°C with IPTG added in ten-fold increments from 0 to 1000 μM, as indicated. Each growth curve shows the means of results from a single experiment and is representative of at least three independent experiments performed in quadruplicate.

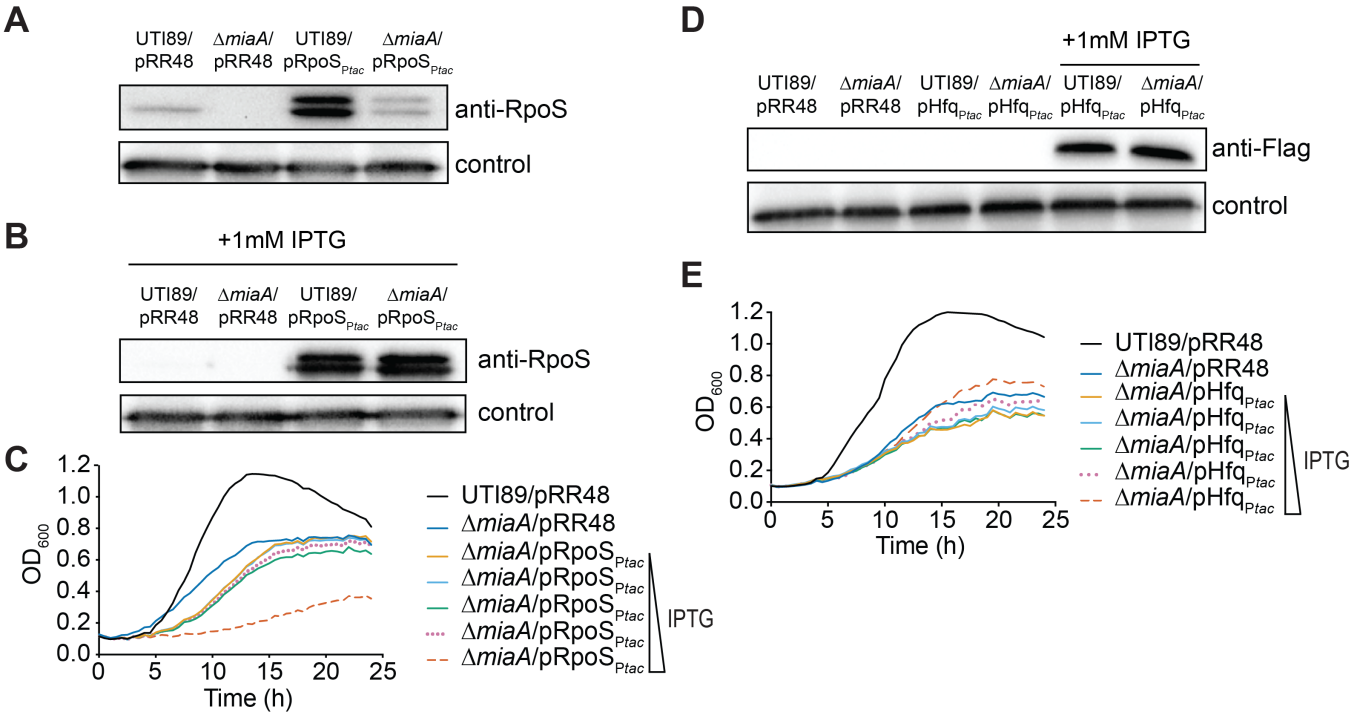

Supplemental Figure S9. Methyl viologen and EDTA alter MiaA levels.

(**A**) Top panel shows schematic of the experimental setup. UTI89/pMiaA-Flag$_{nat}$ was diluted from overnight cultures into fresh LB and grown shaking for 2.5 hours at 37˚C prior to resuspension in LB, LB + 5% NaCl, or LB + 1 mM EDTA. Incubations were continued for another hour before samples were collected and analyzed by western blots.

(**B** and **C**) Blots were probed using anti-Flag (MiaA-Flag) and anti-*E. coli* (loading control, bottom) antibodies.

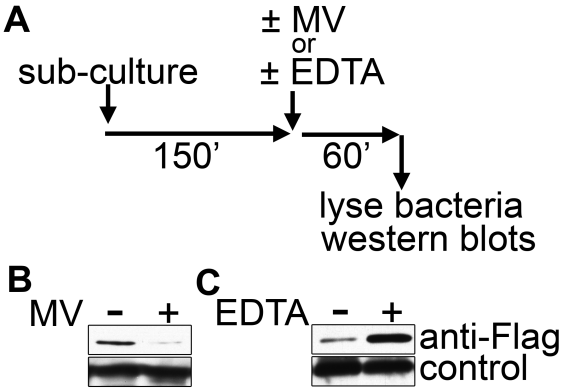

1407 **Supplemental Figure S10. UTI89Δ*miaA* is more sensitive to gentamicin than the**

1408 **wildtype UTI89.**

1409 Bars in graph indicate mean MIC values (± SD) determined from three independent

1410 Etests. *P*-value was determined by an unpaired Student's *t* test.

1411

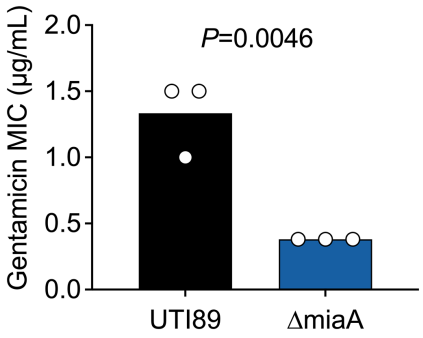

Supplemental Table S1. Bacterial strains and plasmids

Strain or Plasmid	Description	Source or Reference
Strains		
UTI89	UPEC reference strain, cystitis isolate	[52, 108]
UTI89::Kan^R	UTI89 with a Kan^R resistance cassette inserted at the *att*Tn7 site	This study
UTI89Δ*miaA*	UTI89 *miaA::*Cam^R	This study
UTI89Δ*miaB*	UTI89 *miaB::*Cam^R	This study
Plasmids		
pACYC184	Low-copy number plasmid; Tet^R, Cam^R	New England Biolabs
pBAD18	Arabinose-inducible bacterial expression plasmid; Amp^R	[109]
pBAD33	Arabinose-inducible bacterial expression plasmid; Cam^R	[109]
pKD3	Carries FRT-flanked Cam^R cassette; template for use in lambda-Red-mediated recombination	[48]
pKD4	Carries FRT-flanked Kan^R cassette; template for use in lambda-Red-mediated recombination	[48]
pKM208	IPTG-inducible lambda Red recombinase expression plasmid; Amp^R	[49]
pRR48	Contains IPTG-inducible P_{tac} promoter upstream of the MCS; Amp^R	[110]
pHfq$_{Ptac}$	*hfq* from UTI89 cloned with c-terminal 6xHis and FLAG tags into PstI, HindIII sites of pRR48; Amp^R	This Study
pRpoS$_{Ptac}$	*RpoS* cloned from UTI89 into PstI, HindIII sites of pRR48; Amp^R	[62]
pMiaA$_{Ptac}$	*miaA* cloned from UTI89 into PstI, KpnI sites of pRR48; Amp^R	This study
pMiaB$_{Ptac}$	*miaB* cloned from UTI89 into PstI, KpnI sites of pRR48; Amp^R	This study
pMiaA$_{nat}$	*miaA* plus 200 bp of flanking sequences cloned from UTI89 into the EcoR1 site of pACYC184; Tet^R	This study
pMiaA-Flag$_{nat}$	pACYC184-derived plasmid encoding MiaA with N-terminal Flag tag plus linker under control of native *miaA* promoter; Tet^R	This study

p2Luc-HIV	Eukaryotic reporter construct with the HIV *gag-pol* frameshift region inserted between the renilla and firefly luciferase genes. The HIV linker sequence contains a 2-nucleotide insertion resulting in a stop codon located 6 codons after the start of firefly luciferase gene. The firefly gene is in a -1 frame relative to the upstream renilla gene; Amp^R	Derived from [76]
p2Luc-HIV-IF	Control for p2Luc-HIV. The HIV *gag-pol* linker was altered to keep the renilla and firefly luciferases in-frame; Amp^R.	Derived from [76]
p2Lucaz1	Eukaryotic reporter construct with the Az1 frameshift region inserted between the renilla and firefly luciferase genes. The Az1 linker sequence contains a stop codon positioned in-frame so that a +1 frameshift must occur for read-through expression of firefly luciferase; Amp^R	[75]
p2Lucaz1-IF	Control for p2Lucaz1. The Az linker was altered to keep the renilla and firefly luciferases in-frame; Amp^R	[75]
pCWR42-CamR	Dual luciferase reporter with in-frame Az1 linker cloned from p2Lucaz1-IF into pBAD33. Has a Shine-Dalgarno sequence and is under control of the arabinose-inducible P_{BAD} promoter. Control for pCWR43-CamR; Cam^R	This study
pCWR42-AmpR	Dual luciferase reporter with in-frame Az1 linker cloned from p2Lucaz1-IF into pBAD18. Has a Shine-Dalgarno sequence and is under control of the arabinose-inducible P_{BAD} promoter. Control for pCWR43-AmpR; Amp^R	This study
pCWR43-CamR	Dual luciferase reporter with Az1 linker cloned from p2Lucaz1 into pBAD33. Has a Shine-Dalgarno sequence and is under control of the arabinose-inducible P_{BAD} promoter; Cam^R	This study
pCWR43-AmpR	Dual luciferase reporter with Az1 linker cloned from p2Lucaz1 into pBAD18. Has a Shine-Dalgarno sequence and is under control of the arabinose-inducible P_{BAD} promoter; Amp^R	This study
pCWR44-CamR	Dual luciferase reporter with in-frame HIV linker cloned from p2Luc-HIV-IF into pBAD33. Has a Shine-Dalgarno sequence and is under control of the arabinose-inducible P_{BAD} promoter. Control for pCWR45-Cam; Cam^R	This study

pCWR44-AmpR	Dual luciferase reporter with in-frame HIV linker cloned from p2Luc-HIV-IF into pBAD18. Has a Shine-Dalgarno sequence and is under control of the arabinose-inducible P_{BAD} promoter. Control for pCWR45-Amp; Amp^R	This study
pCWR45-CamR	Dual luciferase reporter with HIV linker cloned from p2Luc-HIV into pBAD33. Has a Shine-Dalgarno sequence and is under control of the arabinose-inducible P_{BAD} promoter; Cam^R	This study
pCWR45-AmpR	Dual luciferase reporter with HIV linker cloned from p2Luc-HIV into pBAD18. Has a Shine-Dalgarno sequence and is under control of the arabinose-inducible P_{BAD} promoter; Cam^R	This study

Supplemental Table S2. Primers used in this study

Primer Name[a]	Sequence (5'-3')[b]
Cloning primers	
MiaA-pRR48-F	CGCGCTGCAGATGAGTGATATCAGTAAGGCG
MiaA-pRR48-R	CGGCGGTACCTCAGCCTGCGATAGCACCAAC
MiaB-pRR48-F	CGCGCTGCAGATGACCAAAA AACTCCATAT TAAAACC
MiaB-pRR48-R	CGGCGGTACCGAATTACGGCTGATAATAAC
MiaA-Flag-pACYC184-F	CGGCGAATTCGGCTAAAAGTTTCTGGCGAAGAAAAATCGG
MiaA-Flag-pACYC184-R	CGCGGAATTCCTATCCCTTATCGTCGTCATCCTTGTAGTCT GGTCCTCCTCCTCC GCCTGCGATAGCACCAACAAC
MiaA-pACYC184-F	CGCGGAATTCGCCCCTTAGCCATTCTCTCTTTTCCTTATATG
MiaA-pACYC184-R	CGGCGAATTCCCAGTCCGATGCGCAGCATGTGACCATC
Hfq-pRR48-PstI	CATACCTGCAGATGGCTAAGGGGCAATCTT
Hfq-CFLAG-his-HindII	CATACAAGCTTCTAGTGGTGGTGGTGGTGGTGTCCCTTATC GTCGTCATCCTTGTAGTCTCC TTCGGTTTCTTCGCTGTCCT
p2Luc-F	GCCGGGGTACCAGGAGGTCAGTCAGATGACTTCGAAAGTT TATGATCCAG
p2Luc-R	GCCGGAAGCTTTTACAATTTGGACTTTCCGCCC
Knockout, insertion, and confirmation primers	
*att*Tn7KanR-KI-F	TCTGGCGTAGCCTGGGAGTTATTGCCGGATGCGATGCTGGT GTGTAGGCTGGAGCTGCTTCG
*att*Tn7KanR-KI-R	TCACGTAAAAAAACGTCTAATCCGTAGACCGGATAAGAGGCA TATGAATATCCTCCTTAG
MiaA-KO-F	CGATAAAAGCCCTGAAAGATGAGTGATATCAGTAAGGCTGTG TAGGCTGGAGCTGCTTCG
MiaA-KO-R	CGTCTCCTGACGTTTGCGTCAGTTCCGTTAAAGTTTTACCCAT ATGAATATCCTCCTTAG
MiaA-KO-Conf-F	GCCGCCGGGTGGTCTGTTAC
MiaA-KO-Conf-R	CAGCCTGCGATAGCACCAAC
MiaB-KO-F	CCTGCATTCCTGGCTACTATTTCGCAAGAGCAAGTCGTGTGT AGGCTGGAGCTGCTTCG
MiaB-KO-R	CGGCGGGCCTGAGAATTACGGCTGATAATAACCCACGCCAT ATGAATATCCTCCTTAG
MiaB-KO-Conf-F	GCCGACCATTCCTCCGCCGAC
MiaB-KO-Conf-R	CATTGTCTGCTGGCTCCAGG
RT-qPCR primers	
miaA-F	TACGGACTTGCCTTCCATTC
miaA-R	GCGCAAACACCTCGATAAAC
miaB-F	GTAGAAGGTACATCGCGTAAG
miaB-R	TCGGGTAGACGTCGGTAAT
rpoD-F	TTCGTACGCAAGAACGTCTG
rpoD-R	AGGTATCGCTGGTTTCGTTG

[a] F, forward primer; R, reverse primer; KO, knockout primer; KI, knock-in primer; Conf, confirmation primer. [b] Added restriction sites in cloning primers underlined.